Palaeogeography, Palaeoclimatology, Palaeoecology 598 (2022) 111015

Contents lists available at ScienceDirect

Palaeogeography, Palaeoclimatology, Palaeoecology

journal homepage: www.elsevier.com/locate/palaeo

A multidisciplinary approach to characterise the Early-Middle Holocene palaeoenvironmental evolution of the Sado Valley of Portugal: Implications for late Mesolithic human communities

Ana Maria Costa [a,b,c,d,*], Maria da Conceição Freitas [c,e], Marco A. Jiménez-González [f,g], Nicasio T. Jiménez-Morillo [h], Cristina Barroca Dias [f,i], Cristina Val-Péon [j], Klaus Reicherter [j], Francisco Fatela [c,e], Ana Cristina Araújo [a,b,k], Sónia Gabriel [a,b,k], Manel Leira [l,m], Mariana Diniz [k], Pablo Arias [d]

[a] Laboratório de Arqueociências (LARC)-DGPC, Calçada do Mirante à Ajuda, n° 10A, 1300-418 Lisboa, Portugal
[b] InBIO | Research Network in Biodiversity and Evolutionary Biology (Associate Laboratory) and CIBIO | Research Centre In Biodiversity and Genetic Resources, University of Porto, Portugal
[c] IDL | Instituto Dom Luiz, Universidade de Lisboa, Campo Grande, 1749-016 Lisboa, Portugal
[d] IIIPC (Universidad de Cantabria - Gobierno de Cantabria-Santander), Avda de los Castros 52, 39005 Santander, Spain
[e] Departamento de Geologia, Faculdade de Ciências, Universidade de Lisboa, Campo Grande, 1749-016 Lisboa, Portugal
[f] HERCULES Laboratory, University of Évora, Largo Marquês de Marialva, 8, Évora 7000-809, Portugal
[g] Department of Geology and Geochemistry, Autonomous University of Madrid, Madrid 28049, Spain
[h] MED, Universidade de Évora, Núcleo da Mitra, Ap. 94, 7006-554 Évora, Portugal
[i] Chemistry Department, School of Sciences and Technology, University of Évora, Rua Romão Ramalho, 59, 7000-671 Évora, Portugal
[j] Institute of Neotectonics and Natural Hazards, RWTH Aachen University, Lochnerstraße 4-20, 52060 Aachen, Germany
[k] UNIARQ-Centro de Arqueologia da Universidade de Lisboa, Faculdade de Letras, Universidade de Lisboa, 1600-214 Lisboa, Portugal
[l] BioCost Research Group, Facultade de Ciencias and Centro de Investigacións Científicas Avanzadas (CICA), Universidade de A Coruña, 15071 A Coruña, Spain
[m] Biodiversity and Applied Botany Research Group, Departmento de Botánica, Facultade de Bioloxía, Universidade de Santiago de Compostela, 15782 Santiago de Compostela, Spain

ARTICLE INFO

Editor: Dr. Howard Falcon-Lang

Keywords:
Geoarchaeology
Landscape
Palaeoestuary
Biomarkers
Palynology

ABSTRACT

In this paper we present the results of a multidisciplinary study performed in the Carrasqueira valley, a tributary of the River Sado (SW Portugal), aimed at characterising the Holocene environmental conditions during the late Mesolithic occupation of this valley. Our findings are based on a 13.5 m long sediment core (Arez3) collected on the alluvial plain close to a late Mesolithic shell midden, the Arapouco site. The results of the multiproxy analyses (texture, magnetic susceptibility, organic composition and chemistry, *n*-alkanes and palynology) point to a greater marine influence between ca. 8850 cal yrs. B.P. (at the core base) and ca. 7450 cal yrs. B.P. (at 750 cm below mean sea level (MSL)) and the existence of an environment similar to the present-day central estuarine basin. At this point in time, sedimentation rates were lower than the rate of sea-level rise, resulting in the formation of a drowned area with intertidal environments developing on the less incised margins. After 7040 cal yrs. B.P. the contribution of organic matter from terrestrial plants and freshwater phytoplankton to the sediment increased, reflecting a change in the sedimentary pattern, with the estuarine environments progressively giving way to freshwater environments. After the Middle Holocene (ca. 6530 cal yrs. B.P.), negative shifts of $\delta^{15}N$ to values ~0‰ point to hyper-eutrophication and cyanobacteria bloom episodes under backswamp conditions. According to these results, the estuarine environment prevailed in the area until 7040 cal yrs. B.P. (5090 cal yrs. B.C.; 390 cm below MSL), i.e., during the Mesolithic occupation of the valley, allowing for the occurrence and for the exploitation of marine shellfish and fish by these hunter-gatherer communities at the proximity of the downstream occupation areas.

* Corresponding author at: Laboratório de Arqueociências (LARC)-DGPC, Calçada do Mirante à Ajuda, n° 10A, 1300-418 Lisboa, Portugal.
E-mail address: acosta@dgpc.pt (A.M. Costa).

https://doi.org/10.1016/j.palaeo.2022.111015
Received 3 November 2021; Received in revised form 22 April 2022; Accepted 22 April 2022
Available online 27 April 2022

1. Introduction

During post-glacial sea level rise deeply incised coastal valleys and lowlands in Atlantic Europe (and elsewhere) were flooded by marine water forming extensive estuarine areas and open bays (Freitas et al., 2002, 2003; Boski et al., 2008; Vis et al., 2008; Hijma et al., 2009; Chaumillon et al., 2010; Laermanns et al., 2021). New interfaces between the land and the sea were created offering space, shelter, and rich natural resources - such as typical of those coastal areas - for human populations. Between ca. 8400 and 7000 cal yrs. B.P. (ca. 6400 to 5000 cal yrs. B.C.; Peyroteo-Stjerna, 2020), extensive estuarine areas developed along the lowermost sections of the Tagus and Sado rivers (Portuguese SW Atlantic *façade*), which were occupied by late Mesolithic hunter-gatherer communities (e.g. Arnaud, 1989; Diniz and Arias, 2012; Bicho et al., 2013; Arias et al., 2015, 2017). This strategic location allowed these communities to explore brackish and freshwater environments as well as terrestrial areas for hunting (e.g. Zilhão, 2004), and some authors relate the proximity to the palaeoestuary as an important survival strategy (Arnaud, 2000; Carvalho, 2009).

The late Mesolithic groups are known to have exploited particularly high quantities of marine resources, mainly shellfish (molluscs), leading to the formation of sites known in archaeology as shell middens. In the case of the Sado valley, the formation of these sites resulted from successive accumulation of shells, mostly *Scrobicularia plana* and *Cerastoderma edule* (Gutiérrez-Zugasti et al., 2011), consumed during the Mesolithic stays, as well as other remains related to the exploitation of the aquatic environment, particularly fish bones from coastal waters such as those from *Chelon labrosus*, *Galeorhinus galeus*, *Sparus aurata*, *Argyrosomus regius* and *Dicentrarchus labrax* (Arapouco and Poças de São Bento shell middens, Sado estuary; Gabriel et al., 2012; Gabriel unpub. data). Palaeodiet studies ($\delta^{13}C$ and $\delta^{15}N$) performed on Mesolithic individuals buried in some of these shell midden sites confirm that marine resources were an important food-component of their diet, despite the differences found between the Tagus and Sado groups (Umbelino and Cunha, 2012; Fontanals-Coll et al., 2014; Peyroteo-Stjerna, 2020). Given the relation of late Mesolithic people with the sea and its resources, the reconstruction of the local environment is a key-element to the comprehension of these communities.

The Late Glacial and Holocene palaeoenvironmental conditions of the Tagus estuary have been extensively studied (Vis et al., 2008). Maximum marine flooding occurred ca. 7000 cal yrs. B.P. (Vis et al., 2008), forming a large estuarine area of nearly 1300 km^2 (more than 4 times larger than the present-day estuary) extending for more than 100 km upstream of the present-day estuary inlet (Taborda et al., 2009). Late Mesolithic Tagus shell middens border three tributaries of this river's left margin, namely the Muge, Magos, and Vale da Fonte da Moça rivulets (Arnaud, 1987; Bicho et al., 2013), located up to more than 65 km from the present-day estuary inlet. The lowermost section of these streams was flooded during the Holocene transgression and was part of the extensive estuarine area of the Tagus. The sedimentary record retrieved from the Muge tributary attests the existence of brackish conditions in the area since ca. 8050 cal yrs. B.P., with maximum marine influence between ca. 7750 and ca. 7450 cal yrs. B.P. (van der Schriek et al., 2007, 2008). These conditions gradually transitioned to those of freshwater wetlands, as sea-level rise slowed down, but this only occurred after the abandonment of the sites by late Mesolithic communities, by ca. 6650–5750 cal yrs. B.P. (van der Schriek et al., 2007). Similar to what happened in the Tagus valley, brackish conditions were previously inferred for the section of the Sado valley occupied by these groups (Arnaud, 2000; Diniz and Arias, 2012; Araújo, 2015). The environmental conditions of the Sado valley during the Mesolithic occupation, however, are still poorly known. The present study aimed at characterising the environmental context of the Sado late Mesolithic shell middens in detail. To achieve this we employed a multiproxy approach including sedimentology (grain-size, magnetic susceptibility and coarse fraction composition), organic chemistry (organic quantification, isotopic composition and lipid fraction characterization), palaeoecology (foraminifera and diatoms) and radiocarbon dating, to reconstruct the succession of sedimentary environments recorded in a 13.5 m long sediment core (Arez3) collected in a tributary of the Sado valley, the Carrasqueira stream, located near the most downstream shell midden, Arapouco. In addition, palynological analyses were performed, particularly in the sediments comprising the late Mesolithic occupation, to draw a schematic reconstruction of the environment and landscapes occupied by these groups.

2. Study area

The River Sado is located in southwest Portugal (Fig. 1). It has a maximum length of 175 km and drains a wide watershed area with 7700 km^2 (INE, 2007). It runs northward until the confluence with the Odivelas stream and it bends to northwest further downstream to its mouth, near the city of Setúbal (Fig. 1).

The river has a Mediterranean flow regime with an instantaneous discharge of 1 $m^3\ s^{-1}$ during the dry season and 50 to 80 $m^3\ s^{-1}$ during the rainy season, occasionally reaching 470 $m^3\ s^{-1}$ (Bettencourt and Ramos, 2003 and references therein). The lowermost section of the river corresponds to a bar-built estuary occupying an area of 140–150 km^2 (Bettencourt and Ramos, 2003; Brito, 2009) with a mean depth of 8 m, reaching 44 m near the inlet (Brito, 2009). The estuary is protected by the Tróia sand spit (Fig. 1), a barrier that started to grow northwards at ca. 6500 cal yrs. B.P. (Costas et al., 2015), causing a decreasing exchange of water and sediments between the estuary and the sea. Sado reaches the Atlantic Ocean through a narrow inlet (2 km) between Setúbal and the north of the Tróia spit (Fig. 1). The estuary extends for a length of 50 km considering the maximum salt-water intrusion, or 57 km if the upper limit of the dynamic tide is considered (Bettencourt and Ramos, 2003).

In the studied area, the Sado valley is embedded in pre-Quaternary sediments, mostly belonging to the Palaeocene formation of Vale do Guizo (Fig. 2). The Vale do Guizo Formation is essentially composed of alluvial pinkish sandy conglomerates and marly clays (Antunes et al., 1983; Gonçalves and Antunes, 1992; Pimentel, 2002), limestones cropping out at the top. Near the Xarrama river - one of the tributaries that drains into the study area - the Vale do Guizo Formation comprises a heterogeneous and heterometric conglomerate with carbonate cement (Gonçalves and Antunes, 1992).

The Carrasqueira stream is a tributary of the left margin of the Sado (Fig. 1) and is embedded ca. 15 m in the Palaeocene and Pliocene sedimentary formations of Vale do Guizo and Marateca, respectively (Figs. 2 and 3; Costa et al., 2020). The Marateca Formation mostly comprises orange sands and clays of fluvial origin (Antunes et al., 1991; Gonçalves and Antunes, 1992). Aeolian quartz-rich sands dated from the Pleistocene/Holocene remobilising old sediments also extend over the study area (Gonçalves and Antunes, 1992; Fig. 2).

Several scenarios have been proposed for the Late Glacial sea-level rise in the Portuguese margin (e.g., Dias et al., 2000) and during the Holocene (Teixeira et al., 2005; Vis et al., 2008; Leorri et al., 2012; Costas et al., 2016; García-Artola et al., 2018). In the present work, the model by García-Artola et al. (2018), which is based on 17 index points and 4 marine limiting dates, was used. According to this model, the mean sea level (MSL) rose ca. 34 m (± 1.2 to 1.7 m) between 11,500 and 7500 cal yrs. B.P. (9550 and 5550 cal yrs. B.C.) at a rate of 0.81 ± 0.07 cm yr^{-1}; ca. 0.8 m (±1.7 to 1.2 m) between 7500 and 6900 cal yrs. B.P. (5550 and 4950 cal yrs. B.C.) at a rate of 0.34 ± 0.01 cm yr^{-1}; and, finally the index points indicate a MSL rise from −160 ± 160 cm at ca. 4100 cal yrs. B.P. (2150 cal yrs. B.C.) to −150 ± 150 cm at ca. 1500 cal yrs. B.P. (450 cal yrs. A.D.) at a rate of 0.0 ± 0.05 cm yr^{-1}.

The Carrasqueira rivulet comprises a low energy vertical accreting environment allowing for the characterization of local to regional (mostly based on inferred vegetation changes) environmental conditions and changes due to sea-level rise during the Mesolithic occupation and through the Holocene. Additionally, the Carrasqueira rivulet is close to

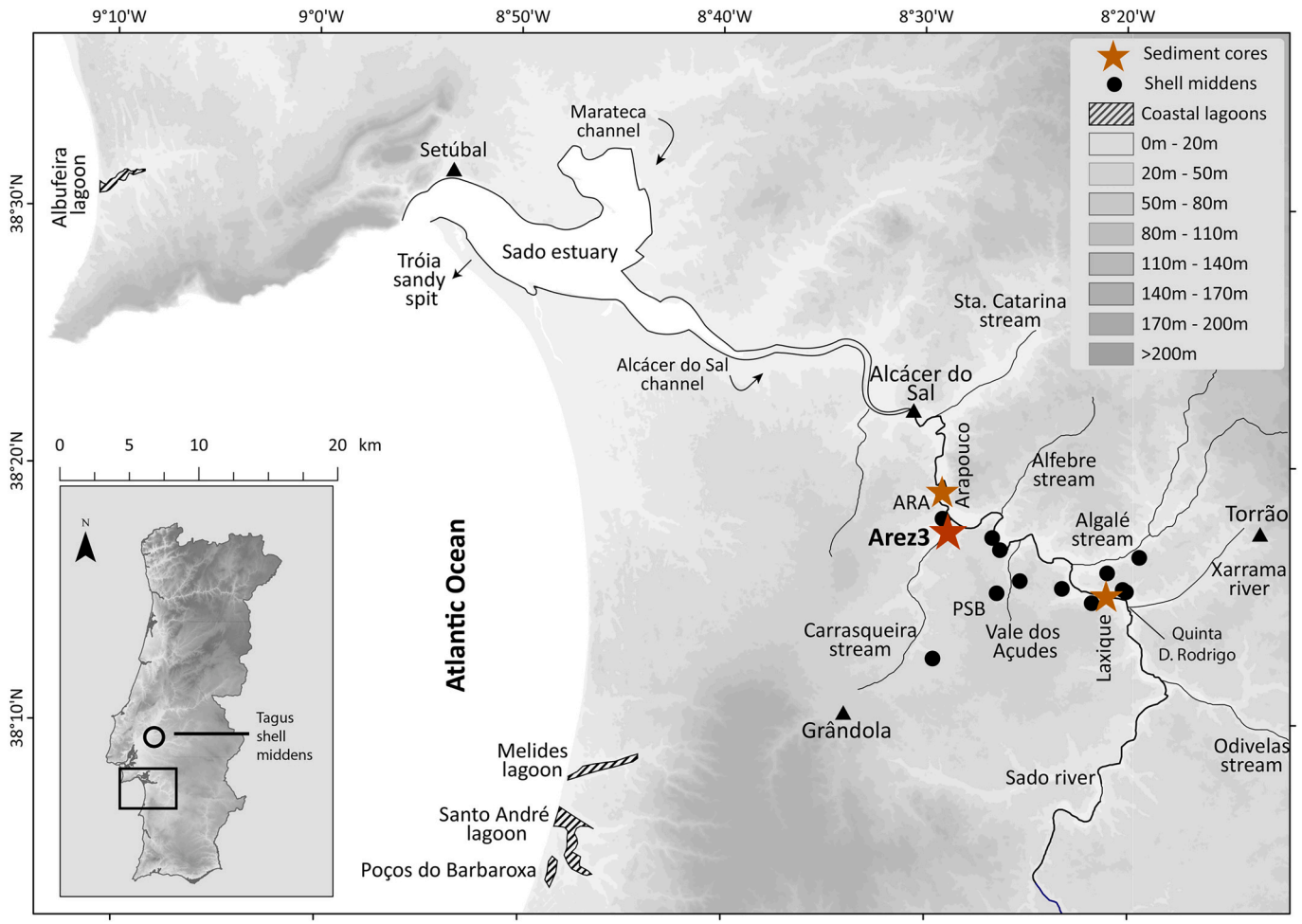

Fig. 1. Studied area with location of the Arez3, Arapouco and Laxique cores, and Late Mesolithic shell middens. ARA - Arapouco; PSB - Poças de S. Bento. Altimetry for Portugal © ESRI Portugal. Location of sediment cores obtained using Leica Geosystems models GPS 900 and NetRover. Location of the shell middens retrieved from Diniz and Arias, 2012.

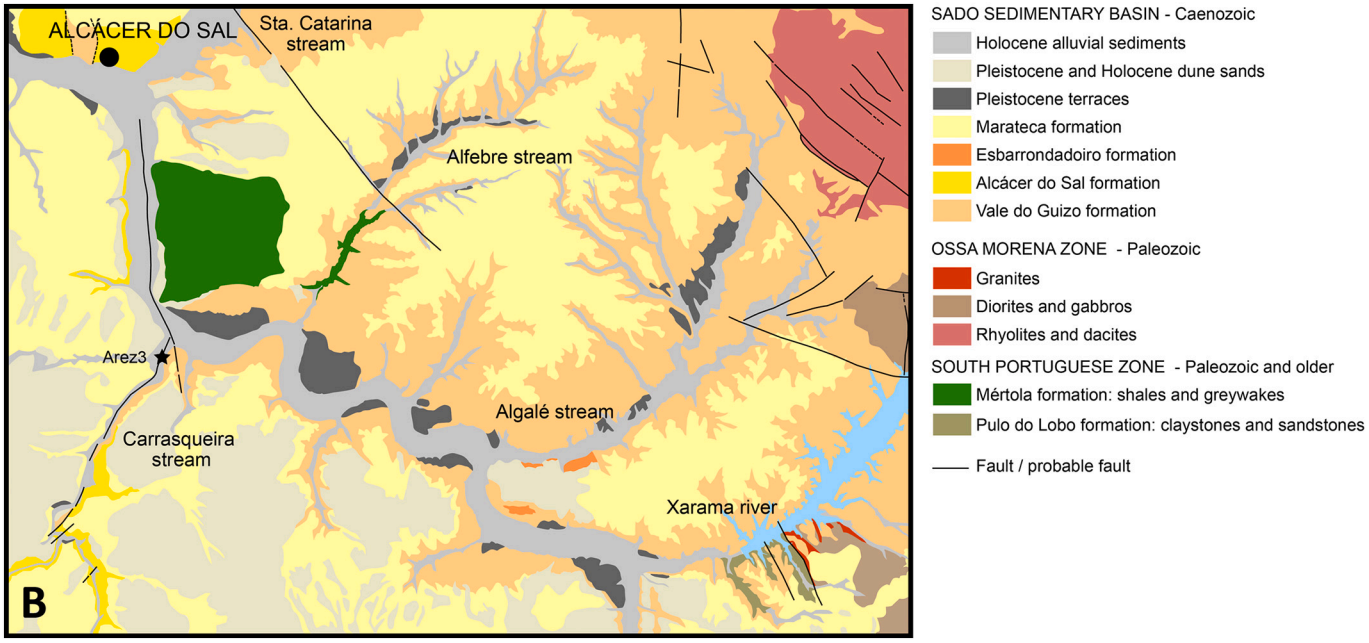

Fig. 2. Geological map of the studied area based on the Geological Map of Portugal 1:50000 39-C, Alcácer do Sal (Antunes et al., 1983), and Geological Map of Portugal 1:50000 39-D, Torrão (Antunes et al., 1991). Adapted from Costa et al., 2020.

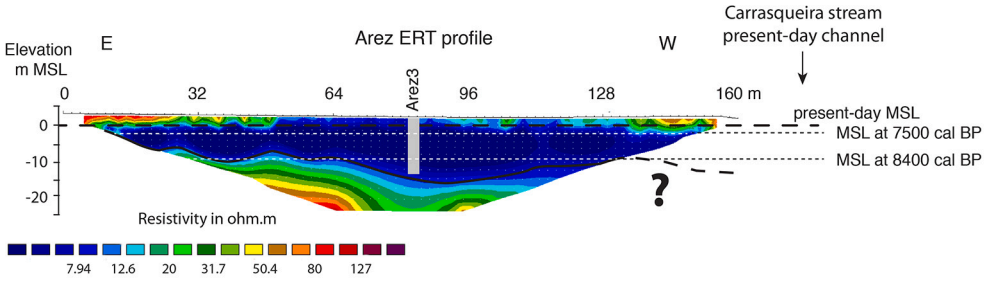

Fig. 3. Carrasqueira palaeomorphology based on the ERT profile and its interpretation and location of Arez3 sediment core. Less resistive sediments (represented in blue) correspond to the Holocene infilling. High resistivity sediments (light blue to red) correspond to Pre-Quaternary sediments of the Lower Sado basin. Black line indicates the maximum incision of the palaeovalley during the Last Maximum Glacial. Detailed information can be found in Costa et al., 2020. (For interpretation of the references to colour in this figure legend, the reader is referred to the web version of this article.)

the most downstream shell midden, at Arapouco (Fig. 1), therefore constituting an excellent site to investigate (using a multiproxy analyses of the valley-filling sedimentary sequence) the environmental conditions of the area during the occupation of the shell middens sites by the last hunter-gatherers of SW Iberia.

Twelve archaeological sites were identified in the lower reaches of the River Sado. Most are located at the top of the steep slopes margining the Sado main river channel and those of its tributaries. and occur scattered through an area of 15 km between Arapouco (50 km upstream the present-day estuary inlet) and Quinta de D. Rodrigo (65 km upstream the present-day estuary inlet) (Araújo, 1997; Arnaud, 2000; Diniz and Arias, 2012; Arias et al., 2015; Fig. 1). As mentioned above, these sites are essentially composed of *S. plana* and *C. edule* shells (Gutiérrez-Zugasti et al., 2011), also displaying remains related to fishery, as attested by the presence of diverse species of fish (e.g. *C. labrosus*, *G. galeus*, *S. aurata*, *A. regius* and *D. labrax*; Gabriel et al., 2012; Gabriel, unpub. data), particularly in Arapouco and Poças de São Bento, as well as testimonies of several other activities.

3. Materials and methods

3.1. Fieldwork

Three sediment cores were collected in the Sado alluvial plain and the Carrasqueira tributary (Table 1). The sedimentary successions of Arapouco (Costa et al., 2019) and Laxique (Costa et al., 2021), collected in the Sado main channel, cover the Middle-Late Holocene transition and the Late Holocene. Arez3, retrieved from the alluvial plain of the Carrasqueira stream in 2018, is the longest (1350 cm) and more complete sedimentary sequence in the area, and for this reason was chosen for the palaeoenvironmental analyses presented here. The sediment core top is located at 290 cm above MSL and reaches a depth of 1090 cm below MSL (coordinates and altimetry obtained using GNSS roving receiver units from Leica Geosystems models GPS 900 and NetRover, operating in real-time, connected to Portuguese internet-based correction services; from now onwards all depths are represented in elevation relative to present-day MSL). The Carrasqueira stream is a tributary of the left margin of the Sado, located 50 km upstream of the river inlet (Fig. 1). The sediment core was collected using a coring device Cobra TT of Atlas Copco and a hydraulic lifting unit using closed PVC tubes.

In addition to Arez3, the basal samples (between −775 and − 798 cm MSL) of a prospecting core (Arez1) collected a few meters downstream from Arez3, were analysed for organic chemistry, diatom assemblages, and chronology and are here presented (detailed results in Costa et al., 2020).

3.2. Sediment sampling

In the laboratory, Arez3 core was opened, described and sub-sampled every 2 cm. Sediment sub-samples were subsequently freeze-dried, split, and a representative quantity was grinded using an agate mill.

3.3. Radiocarbon dating

Eight organic samples from Arez3 and one organic sample from Arez1 (Table 2) were selected for AMS radiocarbon dating and processed at Beta Analytic (USA) and A.E. Lalonde AMS (Canada) laboratories following the analytical procedures specific of each laboratory (which can be accessed at https://www.radiocarbon.com/beta-lab.htm and Crann et al. (2017), respectively). In the case of A.E Lalonde lab, the errors on ^{14}C ages (1σ) are based on counting statistics and $^{14}C/^{12}C$ and $^{13}C/^{12}C$ variation between data blocks. As $^{12,13,14}C$ isotopes are measured online and corrections done during the procedure, $\delta^{13}C$ measurements are not reported. Radiocarbon ages determined for the organic samples were calibrated using the IntCal20 calibration curve (Reimer et al., 2020). Sedimentation rates were extrapolated using the linear interpolation of CLAM 2.3.2 software (Blaauw, 2010).

3.4. Magnetic susceptibility

Volume magnetic susceptibility (MS) was measured in SI units directly over the core at every 2 cm using a Bartington® MS2 instrument equipped with a MS2E surface scanner. Measured values were corrected for drift using the Bartington's equipment drift correction.

Table 1
Location and altimetry of the sediment cores. Coordinate are referenced to PT-TM06/ERTS89 coordinate system. Elevations given in relation to mean sea level (MSL).

Location	Core reference	Easting	Northing	Elevation of ground surface at core location	Collected core length	Collection date
Sado channel	Arapouco 2/3	−31,030,6767	−149,673.241	2.2	738 cm	November 2013
	Laxique1	−21,174.326	−157,053.121	6.1	810 cm	November 2015
Carrasqueira stream	Arez3	−30,473.2	−15,279	2.9	1350 cm	March 2018
	Arez1	−30,449.923	−152,111.168	2.7	Only the basal 23 cm were collected	July 2012

Table 2
Radiocarbon determinations on bulk organic sediment from the cores used in this work. The dates have been calibrated with the IntCal20 curve (Reimer et al., 2020) using the Oxcal v.4.4 (© Bronk Ramsey, 2020). Best-fit age was determined based on the age-model draw using CLAM 2.3.2 software (Blaauw, 2010). Grey shaded line refers to the radiocarbon dating from other core, Arez 1, collected few meters downstream Arez3, at an elevation of −842.5 cm MSL (date and location information previously published in Costa et al., 2020 and Table 1).

Sample reference	Lab code	Core depth (cm)	Elevation (cm MSL)	$\delta^{13}C$ (‰)	Conventional ^{14}C age BP	Calibrated age cal yrr B.P.	Calibrated age AD / BC (95%)	Best-fit age cal yrs B.P.
Arez3#3 176-178	UOC -13332	177.5	112.5	-	1239±33	1271-1204 (38.4%) 1191-1070 (57.1%)	680-746 (38.4%) AD 759-880 (57.3%) AD	1216
Arez3#4 300-302	Beta - 582891	301	-11	-23.3	6080±30	7153-7130 (5.2%) 7010-6848 (88.1%) 6815-6800 (2.1%)	5204-5181 (5.2%) BC 5061-4899 (88.1%) BC 4866-4851 (2.1%) BC	6942
Arez3#5 360-362	UOC - 13333	361	-71	-	5965±33	6893-6726 (90.6%) 6707-6676 (4.9%)	4944-4777 (90.6%) BC 4758-4727 (4.9%) BC	6799
Arez3#8 746-748	UOC -10286	746.5	-456.5	-	6231±69	7281-6947 (95.4%)	5332-4998 (95.4%) BC	7120
Arez3#8 786-788*	UOC - 13334	787	-497	-	6011±30	6944-6781 (92.1%) 6765-6749 (3.3%)	4995-4832 (92.1%) BC 4816-4800 (3.3%) BC	-
Arez3#11 966-968	Beta - 582890	967	-676	-25.7	6550±30	7561-7541 (6.8%) 7511-7422 (88.7%)	5612-5592 (6.6%) BC 5562-5473 (88.7%) BC	7464
Arez3#13 1216-1218	UOC - 13335	1217	-927	-	7787±33	8636-8614 (5.3%) 8608-8512 (77.3%) 8503-8455 (12.8%)	6687-6665 (5.3%) BC 6659-6563 (77.3%) BC 6554-6506 (12.8%) BC	8558
Arez3 1348-1349	Beta - 510624	1348.5	-1058.5	-25.2	7970±30	8992-8716 (89.8%) 8709-8699 (1.5%) 8671-8650 (4.1%)	7043-6767 (89.8%) BC 6760-6750 (1.5%) BC 6722-6701 (4.1%) BC	8846
Arez1 1062-1063	Beta - 343145	1062.5	-842.5	-25.9	7810±40	8716-8710 (0.4%) 8699-8670 (3.2%) 8650-8510 (84.5%) 8505-8454 (7.3%)	6767-6761 (0.4%) BC 6750-6721 (3.2%) BC 6701-6561 (84.5%) BC 6556-6505 (7.3%) BC	-

* sample not used in the age-model.

3.5. Grain-size and morphoscopic analyses

The relative percentages of coarse (CF; >63 μm) and fine fractions (FF; <63 μm) were analysed by wet sieving using a standard 63 μm mesh. Samples were characterised following the methodology established by Flemming (2000). The coarse fraction is low (<2% in all Units, except for Unit 3; see Results section), and so it was qualitatively described in terms of composition and morphoscopic characteristics, using a Leica MZ12 binocular stereomicroscope.

3.6. Foraminiferal assemblages

Seven sub-samples from Unit 1 (collected at −977, −887, −827, −797 and − 777 cm MSL) and Sub-unit 2A (−657 and − 617 cm MSL) were analysed for foraminiferal assemblages. Sediment samples were washed with tepid tap water through a 63 μm sieve to remove clay and silt material. The sieve was immersed in a methylene blue solution before each washing to prevent contaminations. The washing residues (CF) were dried in an oven under $T < 50$ °C, to ensure the preservation of tests. After drying, the samples were split to obtain the aliquot statistically representative of each sample, where the presence of at least 100 individuals is estimated, given that this counting is adequate to characterise the low diversity assemblages (Fatela and Taborda, 2002). Foraminiferal collection and identification were performed under a stereo microscope Olympus SZX16, following Loeblich Jr. and Tappan (1988) for the generic classification and other dedicated publications for specific classification (e.g. Murray, 2006; Debenay, 2012). The picked specimens of each sample were archived in the respective micropalaeontological Plummer cell slide. Foraminiferal density (Nf/g; Nf = specimens) was estimated and the assemblage diversity of each sample was measured using the Shannon Index (Shannon, 1948). The species were considered dominant when they represent >10% of the assemblage along the same unit, subsidiary when they do not reach >10%, minor when they correspond to <10% (Murray, 2007).

3.7. Calcium carbonate contents

Calcium carbonate contents (% $CaCO_3$) were determined using an Eijkelkamp calcimeter that measures the CO_2 produced by the reaction of sample calcium carbonate with HCl 4 mol in a known sample mass.

3.8. Organic geochemistry analysis

3.8.1. Quantification and isotopic characterization of organic matter

Total organic matter (OM) content was determined following the adapted method *Loss on ignition* (LOI) by Kristensen (1990): samples were heated in a muffle furnace at 520 °C for 6 h and OM_T was determined by weight difference.

Total organic carbon (% C_{org}), total nitrogen (% N), $\delta^{13}C_{VPDB}$ and $\delta^{15}N_{AIR}$ were determined in grinded sub-samples after removal of inorganic carbon using HCl 10%. Samples were processed at *Servizos de Apoio a Investigación*, University of A Coruña (UDC) - Spain, and at the Stable Isotopes and Instrumental Analysis Facility from Ciências, ULisboa (FCUL). Samples were homogenised and weighed into tin capsules. Capsulated samples were analysed with a FlashEA1112 combustion elemental analyser (ThermoFinnigan) coupled on−line with a Delta Plus Finnigan MAT Isotope Ratio Mass Spectrometer (UDC) and a Sercon Hydra 20–22 (Sercon, UK) stable isotope ratio mass spectrometer,

coupled to a EuroEA (EuroVector, Italy) elemental analyser for online sample preparation by Dumas-combustion (UL). All carbon and nitrogen isotope ratios are expressed in conventional δ notation: $\delta^{13}C_{VPDB}$ and $\delta^{15}N_{AIR}$ calculations are given as $[(R_{sample} - R_{standard})/R_{standard}]*1000$, where R_{sample} and $R_{standard}$ are the $^{13}C/^{12}C$ or $^{15}N/^{14}N$ isotope ratios of the sample and standard, respectively. The $\delta^{13}C$ isotope ratio of samples was determined by comparison with a CO_2 reference gas standard (99.996%, $\delta^{13}C_{VPDB} = -6.317$) and values are reported relative to the Vienna Pee Dee Belemnite (VPDB) standard. $\delta^{15}N$ values are referred to air.

Quality assurance in UDC is made by the measure of duplicate samples while at UL the reference materials USGS-25, USGS-35, BCR-657 and IAEA-CH7 (Coleman and Meier-Augenstein, 2014) were used. The used laboratory standard was Protein Standard OAS/Isotope (Elemental Microanalysis, UK). Uncertainty of the isotope ratio analysis, calculated using values from 6 to 9 replicates of laboratory standard, interspersed among samples in every batch of analysis, was ≤0.1‰. The major mass signals of N and C were used to calculate total N and C abundances, using Protein Standard OAS (Elemental Microanalysis, UK, with 13.32% N, 46.5% C) as elemental composition reference material.

3.8.2. *Molecular characterization of lipid fraction*

The alkane composition of the sediment organic matter was analysed using the analytical pyrolysis technique (Py-GC/MS) applied directly to bulk sediment samples grinded to fine powder (< 0.01 mm). The samples (15–20 mg) were pyrolysed using single shot at 500 °C for 1 min. In the case of interface, a temperature of 280 °C was used. The analytical instrument consisted of a micro-furnace type double-shot pyrolyser (Frontier Lab PY-3030D) coupled to a gas chromatograph (Shimadzu GC2010) fitted with a low polar-fused silica capillary column (Phenomenex Zebron-ZB-5HT Inferno, 30 m length, 0.25 mm internal diameter, 0.50 μm film thickness). The splitless injector operated at a temperature of 250 °C. The GC oven temperature was set at 50 °C for 1 min, then increased to 100 °C at a rate of 30 °C min^{-1}, from 100 to 300 °C at a rate of 10 °C min^{-1}, and finally isothermal at 300 °C for 10 min. The total analysis time corresponded to 32 min. Helium was used as carrier gas at a flow rate of 1 cm^3 min^{-1}.

The mass spectra were acquired using a quadrupole mass spectrometer (Shimadzu GCMS-QP2010) working at negative electronic ionisation mode. In the mass spectrometer, the acquisition of data ranged between 45 and 700 *m/z*. The ion 85 trace was used to identify and quantify the homologous series of alkanes by comparison with the Libraries NIST and Wiley. The peak areas (total ion 85 area counts) in the chromatogram were integrated and expressed as percentage (%) of total abundances. Analytical pyrolysis analyses were done in samples from the transitions between the defined sedimentary units within the core to help better identify the transition.

Different sources of natural organic matter are frequently distinguished by changes in specific n-alkane ratios (e.g. Li et al., 2020). In the present study the Carbon preference index (CPI), P_{aq}, Terrigenous/aquatic ratio (TAR), Terrestrial-marine discriminate index (TMD), Pr/Ph, Pr/C_{17} and Ph/C_{18} ratios were applied (Table 3).

Table 3
n-Alkane ratios used in this work as proxies to distinguish the different sources of natural organic matter.

Name	*n*-alkane ratios	description	diagnostic values	references
Carbon preference index (CPI)	$CPI^{*} = \frac{\sum_{odd} C_n}{\sum_{even} C_n}$	estimates the relative abundance of odd to even C chain numbers and allows discerning different sources of organic matter	<1: bacterial, algal and degraded OM input to the soil/sediments ~1: petrogenic or marine 5–10: terrestrial	Bray and Evans, 1961
P_{aq}	$P_{aq} = \frac{(C_{23} + C_{25})}{(C_{23} + C_{25} + C_{29} + C_{31})}$	distinguishes terrestrial and aquatic plants with mid-length *n*-alkane chains in terrestrial lacustrine environments or coastal environments with freshwater inputs	0.01–0.25: terrestrial plants 0.4–0.6: emergent aquatic plants (including mangroves) >0.6: submerged aquatic plants (including marine macrophytes)	Ficken et al., 2000 Sikes et al., 2009
Terrigenous/aquatic ratio (TAR)	$TAR = \frac{(C_{27} + C_{29} + C_{31})}{(C_{15} + C_{17} + C_{19})}$	distinguishes the relative contributions between land plants (represented by C_{27}, C_{29} and C_{31} *n*-alkanes) and algal inputs (represented by C_{15}, C_{17} and C_{19} *n*-alkanes)	>4: terrigenous <1: aquatic	Silliman et al., 1996; Meyers, 2003
Terrestrial-marine discriminate index (TMD)	$TMD = \frac{(C_{25} + C_{27} + C_{29} + C_{31} + C^{*}_{33})}{(C_{15} + C_{17} + C_{19} + C_{21} + C_{23})}$	distinguishes organic matter from terrestrial (represented by C_{25}, C_{27}, C_{29}, C_{31} and C_{33} n-alkanes) and marine (represented by C_{15}, C_{17}, C_{19}, C_{21} and C_{23}) sources * not measured in the analysed samples	>1: dominant terrestrial input 1: equal inputs from terrestrial and marine sources 0.5: dominant marine contribution 0.5–1: mixed contribution between marine and terrestrial sources	Elfadly et al., 2017
			<1: anoxic environments 1: alternated oxic and anoxic conditions >1: oxic conditions	Hughes et al., 1995
Pristane/Phitane (Pr/Ph)	Pr/Ph	estimates the origin of the organic matter and its maturity	0.8–2.5: most organic-rich marine sediments <1–3: marine oils and sediments >3: input from terrestrial organic matter 5–10: higher plants	Powell, 1988 Mita and Shimoyama, 1999
Pristane/n-alkane C_{17} and Phitane/n-alkane C_{18}	Pr/C_{17}; Ph/C_{18}	often used to indicate the extent of biodegradation of n-alkanes; significant depletion of n-alkanes leads to an increase in these two ratios	higher values point to higher organic matter degradation	e.g. Wang et al., 2008

* $\sum_{odd} C_n$ and $\sum_{even} C_n$ correspond to the total carbon numbers of odd-carbon-chain and even-carbon-chain alkanes in the sediment samples, respectively.

A discriminant analysis was carried out to check how the distribution of the *n*-alkanes could be reflecting information about the different sedimentary units. For the analysis, the abundance of the alkanes detected by analytical pyrolysis was normalised by equalling the sum of the peak of areas of the alkanes to 100 in Microsoft Excel. In this treatment, the relative abundances of the different alkanes were used as descriptors (independent variables). On the other hand, the dependent variables (sedimentary units) consisted of the different layers selected according to the previous textural and chemical analysis. The software Statgraphics Centurion XVI.II was used for this analysis.

3.9. Palynological analyses

Eight sub-samples concentrated at the base of the sedimentary sequence (collected at −1027, −957, −927, −837 and −817 cm MSL from Unit 1, −597 and −417 cm MSL from Sub-unit 2A and −135.5 cm MSL from Sub-unit 2B) were analysed for its palynological content to characterise vegetation and landscape during the late Mesolithic. Sediment at −135.5 cm MSL were also analysed with the purpose of identifying greater changes in the landscape; our analysis for this period, however, cannot be considered exhaustive as it is only based on one sample. All samples were chemically treated with HCl (10%) to remove carbonates, KOH (10%) to remove humic acids, and Sodium Polytungstate (SPT: $3Na_2WO_4{\cdot}9WO_3{\cdot}H_2O$) at 2.0–2.1 cm^3 g^{-1} for densimetric separation. The final residue obtained after the treatment was mounted on slides with the use of glycerol mixed with phenol. Palynomorphs were counted using an optical microscope at 400× and 1000× to a minimum pollen sum of 300 terrestrial pollen grains. Fossil pollen grains, spores, and non-pollen palynomorphs were identified using published keys (van Geel, 1978, 1986, 1992; van Geel et al., 1981, 1989, 2003, 2011; van Geel, 2006; Pals et al., 1980; Jarzen and Elsik, 1986; Moore et al., 1991; Reille, 1992, 1995; Scott, 1992; López-Sáez et al., 2000; Miola, 2012). Microcharcoal particles ≥120 μm and <120 μm were counted alongside the identification of pollen grains and interpreted as indicators of local and regional fires, respectively (Whitlock and Larsen, 2001). Pollen and microcharcoal concentrations (grains gr^{-1} and particles gr^{-1} of dry sediment, respectively) were estimated by adding two *Lycopodium clavatum* tablets for each sample (Stockmarr, 1971). Palynological diagrams were plotted against age using TiliaIT software (version 2.1.1, Illinois State Museum, Research and Collection Center, Springfield USA). Pollen percentages for terrestrial taxa were calculated against the main sum of terrestrial grains, while percentages for aquatics and spores were calculated against the total sum of all pollen and spores.

4. Results

4.1. Chronology and age-model

Table 2 shows the results of radiocarbon dating for Arez3 and Fig. 4 displays the age-model for the sediment core. Older samples yielded dates of ca. 8800 cal yrs. B.P. covering a 13 m long Holocene sedimentary succession. Almost all dates are consecutive revealing a coherent age-model (Fig. 4). The dates obtained for samples

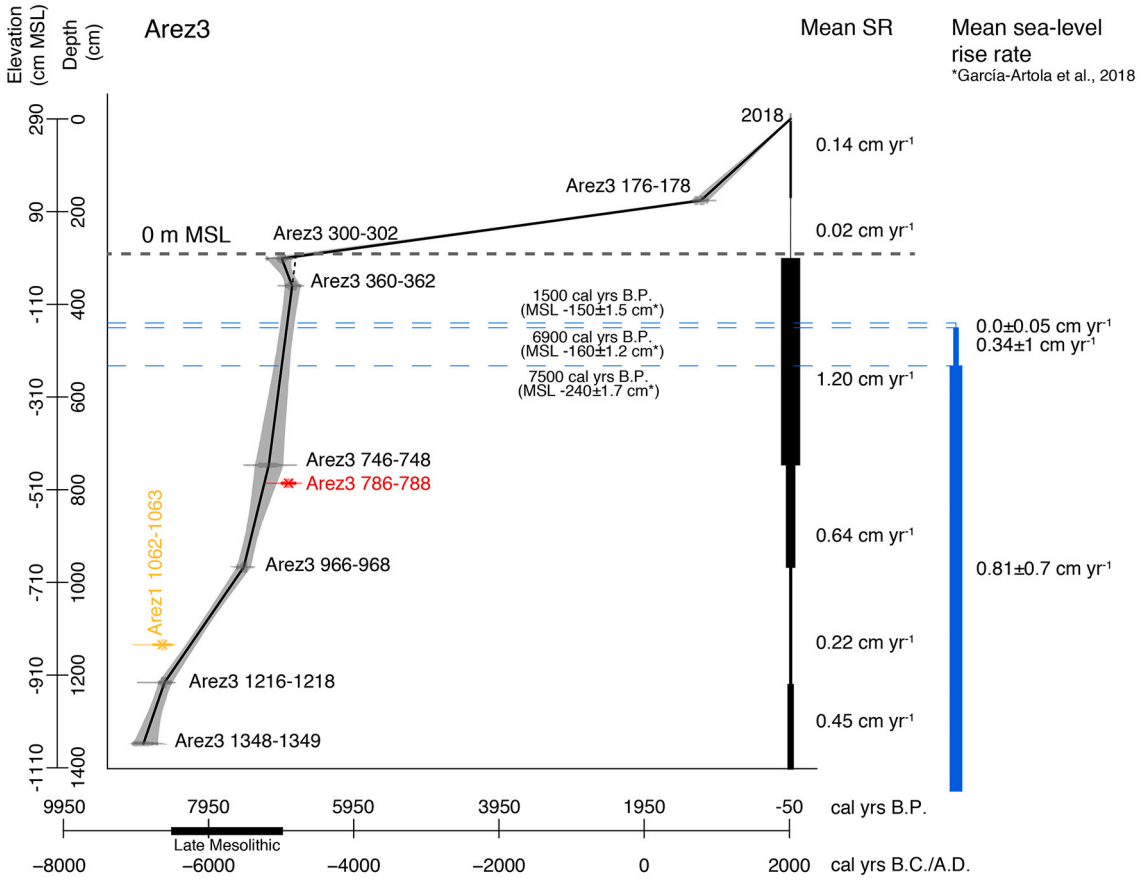

Fig. 4. Age-model and sedimentation rates (SR) determined for Arez3. Sample Arez3 786–788 (in red) was not used for the age-model. Radiocarbon dating of the base of the core Arez 1 core (at −796 cm MSL), collected few meters downstream Arez3 is presented in yellow. Age-model draw using linear interpolation and CLAM 2.3.2 (Blaauw, 2010). Dashed blue lines correspond to the mean sea level at 7500, 6900 and 1500 cal yrs. B.P. according to García-Artola et al., 2018 and assuming a MSL rise rate as determined by the same author (represented in the vertical blue line). (For interpretation of the references to colour in this figure legend, the reader is referred to the web version of this article.)

Arez3#4300–302 and Arez3#8786–788 imply small inversions in relation to the samples collected just below. However, the error associated with the dates is within the limits of the age-model. Even so, the dating of the sample Arez3#8786–788 was considered an outlier and was not used for the age-model (red mark in Fig. 4). According to the model settings, the goodness of fit was 8.6 considering all dates used (7) and the model was accepted. Ages and uncertainty ranges for each date were calculated for each cm and best-fit dates were used for the presentation of the results and interpretations.

Variable and high sedimentation rates (SR) were determined for Arez3 between the base of the core, at −1060 cm MSL and the present-day MSL, following the SR pattern achieved in other cores retrieved in the Sado valley (Costa et al., 2019; Costa et al., 2021). The highest SR of 1.2 cm yr^{-1} was determined for the section between −456.5 and − 10 cm MSL corresponding to the interval between 7120 and 6800 cal yrs. B.P. (i.e. 5170 and 4850 cal yrs. B.C.). The lowest SR of 0.02 cm yr^{-1} was determined above present-day MSL and 177 cm above MSL, corresponding to the interval between 6800 and 1170 cal yrs. B.P. (i.e. 4850 cal yrs. B.C. and 780 cal yrs. A.D.). SR increases in the top 180 cm to values of 0.14 cm yr^{-1}, i.e. for the last ca. 780 years, probably affected by agriculture procedures (discussed below).

4.2. Sedimentary and geochemical characterization

Based on noticeable changes in the analysed proxies, three sedimentary units were identified in the Arez3 core (Figs. 5 and 6). The interval of deposition for each unit was determined considering the proposed age-model and presented in cal yrs. B.P. and cal yrs. B.C./A.D. to better relate data with both environmental and archaeological information. Organic geochemistry results are resumed in Table 4 (. Calcium carbonate results indicate null or negligible amounts (< 1.5% on the analysed samples).

Unit 1 (−1060 to −677 cm MSL; 8850 to 7450 cal yrs. B.P.; 6900 to 5500 cal yrs. B.C.) is constituted by mud and slightly sandy mud with high contents of OM (>5%), organic carbon (> 1.2% with exception of 2 values lower than 1%) and nitrogen (> 0.1%; Fig. 6). The CF is low (mostly <10%). The coarse material essentially comprises heterometric, fine to medium, quartz grains, shell (gastropods) and shell fragments (e.g. *S. plana*?, *Cerastoderma* sp.?, gastropods) and macro plant remains (Fig. 7A). Usually, quartz grains predominate when the sediment is coarser, and plant remains are dominant when the CF has lower %. Frequent foraminifera and rare ostracod valves were identified between −977 and − 777 cm MSL (Fig. 7E). Foraminiferal assemblages exhibit a Nf/g from 12 to 269 and a H(s) of 1.10 and 1.39. *Haynesina germanica* (40 to 57%), *Ammonia tepida* (6 to 27%) and *Elphidium gunteri/oceanensis* (21 to 16%) are the dominant species, followed by the minor

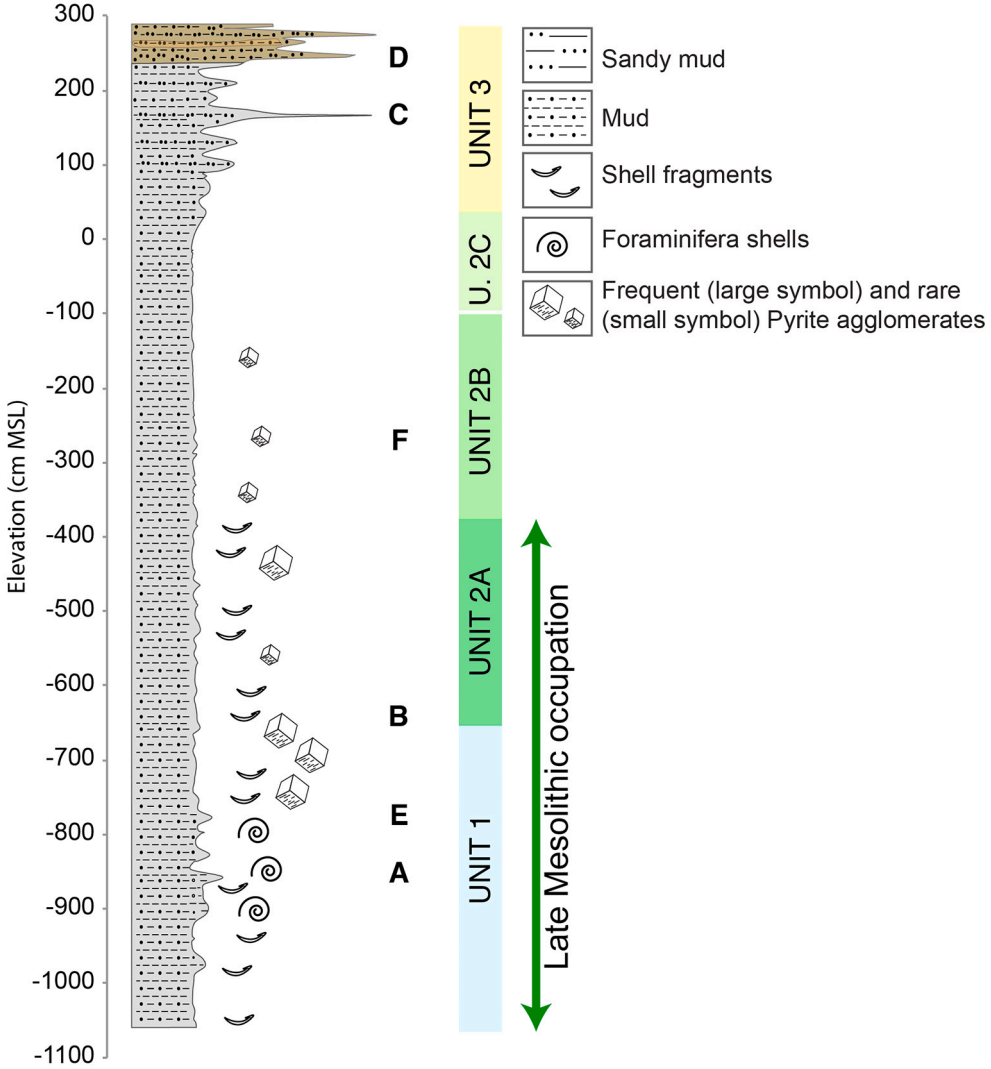

Fig. 5. Arez 3 LOG and representation of coarse fraction principal constituents. Letters in the profile correspond to the CF photos presented in Fig. 7.

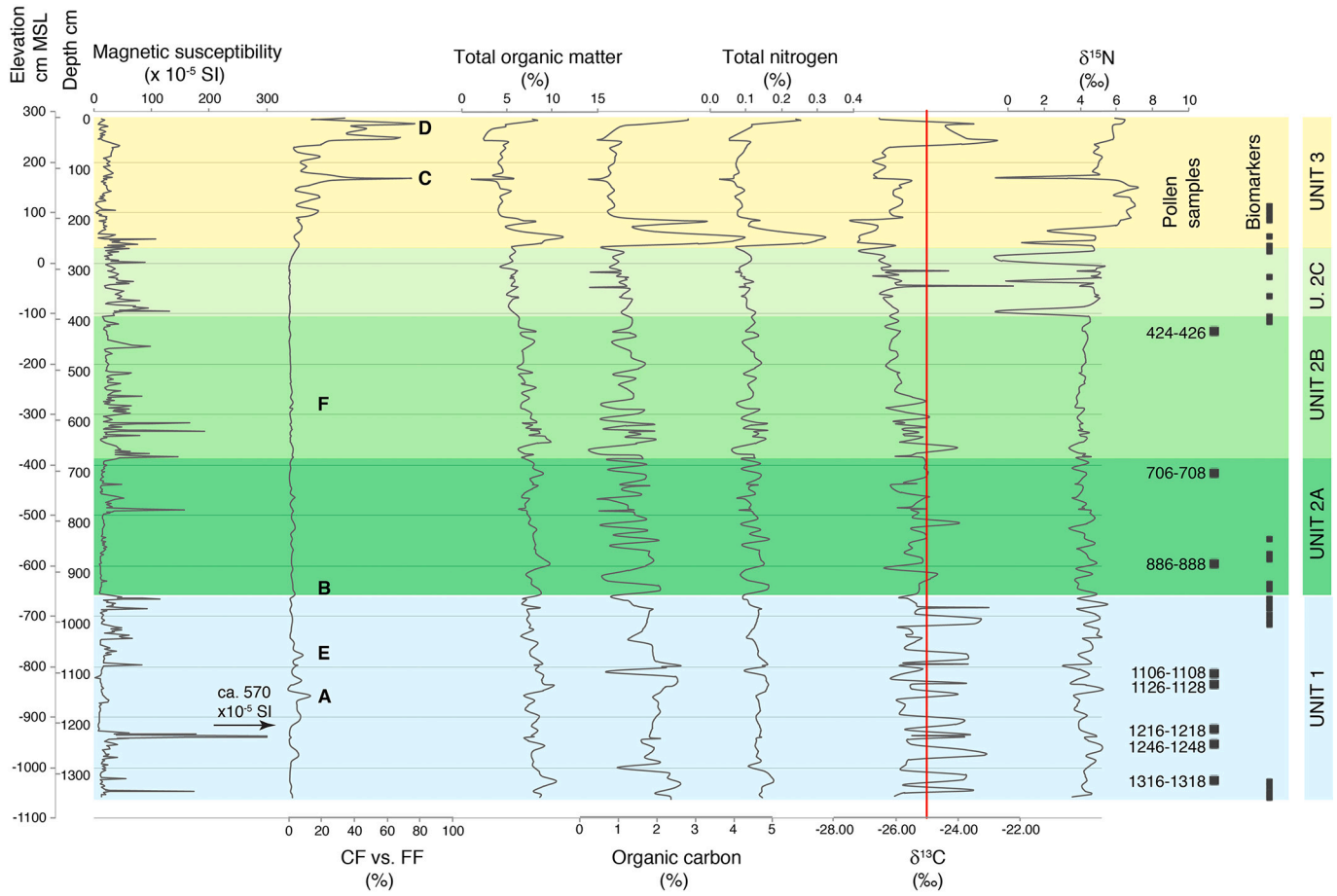

Fig. 6. Representation of sedimentological and organic proxies against elevation cm MSL and depth cm: magnetic susceptibility (MS), texture (CF vs. FF), total organic matter (OM), organic carbon (C_{org}), total nitrogen (N), $\delta^{13}C$ and $\delta^{15}N$. The red line in the $\delta^{13}C$ profile represents the −25‰ value, the limit that usually is used to distinguish between terrestrial/freshwater and marine organic materials (e.g. Lamb et al., 2006; Khan et al., 2015). Letters in texture in-depth profile correspond to the CF photos presented in Fig. 7. (For interpretation of the references to colour in this figure legend, the reader is referred to the web version of this article.)

Table 4
Statistic parameters (mean values) considering the organic geochemistry results: organic carbon (C_{org}), total nitrogen (N), C/N, $\delta^{13}C$ and $\delta^{15}N$; and diagnostic *n*-alkane ratios: Carbon Preference Index (CPI), Terrigenous/aquatic ratio (TAR), Terrestrial-marine discriminate index (TMD), Pristane (Pr) over Phytane (Ph) ratio (Pr/Ph), Pristane to *n*-alkane C_{17} (Pr/C_{17}) and Phytane to *n*-alkane C_{18} (Ph/C_{18}).

		UNIT 1	SUB-UNIT 2A	SUB-UNIT 2B	SUB-UNIT 2C	UNIT 3
Quantification and isotopic characterization of organic matter	C_{org} (%)	1.90	1.32	1.25	1.01	1.37
	N (%)	0.14	0.12	0.12	0.10	0.12
	C/N	13.83	10.84	10.38	10.38	11.30
	$\delta^{13}C$ (‰)	−24.95	−25.35	−25.74	−26.01	−25.92
	$\delta^{15}N$ (‰)	4.37	4.15	4.11	3.90	5.36
Diagnostic *n*-alkanes ratios	CPI	1.08	1.13	0.99	1.05	0.97
	P_{aq}	0.78	0.80	0.75	0.72	0.72
	TAR	0.11	0.09	0.04	0.13	0.33
	TMD	1.31	1.39	1.37	1.26	1.17
	Pr/Ph	0.44	0.55	0.52	1.04	0.87
	Ph/C_{18}	0.47	0.57	0.81	0.21	0.32
	Pr/C_{17}	0.29	0.42	0.48	0.29	0.15

Anomalinoides cf. *globosus* (0 to 13%) and *Ammonia aoteana* (0 to 5%). Additionally, juvenile specimens of planktonic and marine benthic foraminifera (e.g. *Bolivina* spp., *Fissurina* spp.) are also present. Above −746 cm MSL, pyrite is frequent together with quartz and pyritized macro plant remains (Fig. 7F). Magnetic susceptibility is low, but several peaks with higher MS values were measured, including a peak ca. -940 cm MSL that reaches values of 570×10^{-5} SI, the highest value of all the sedimentary column (Fig. 6). $\delta^{13}C$ is quite variable in this unit, varying constantly between maximum values of −23‰ and minimum values of −26‰.

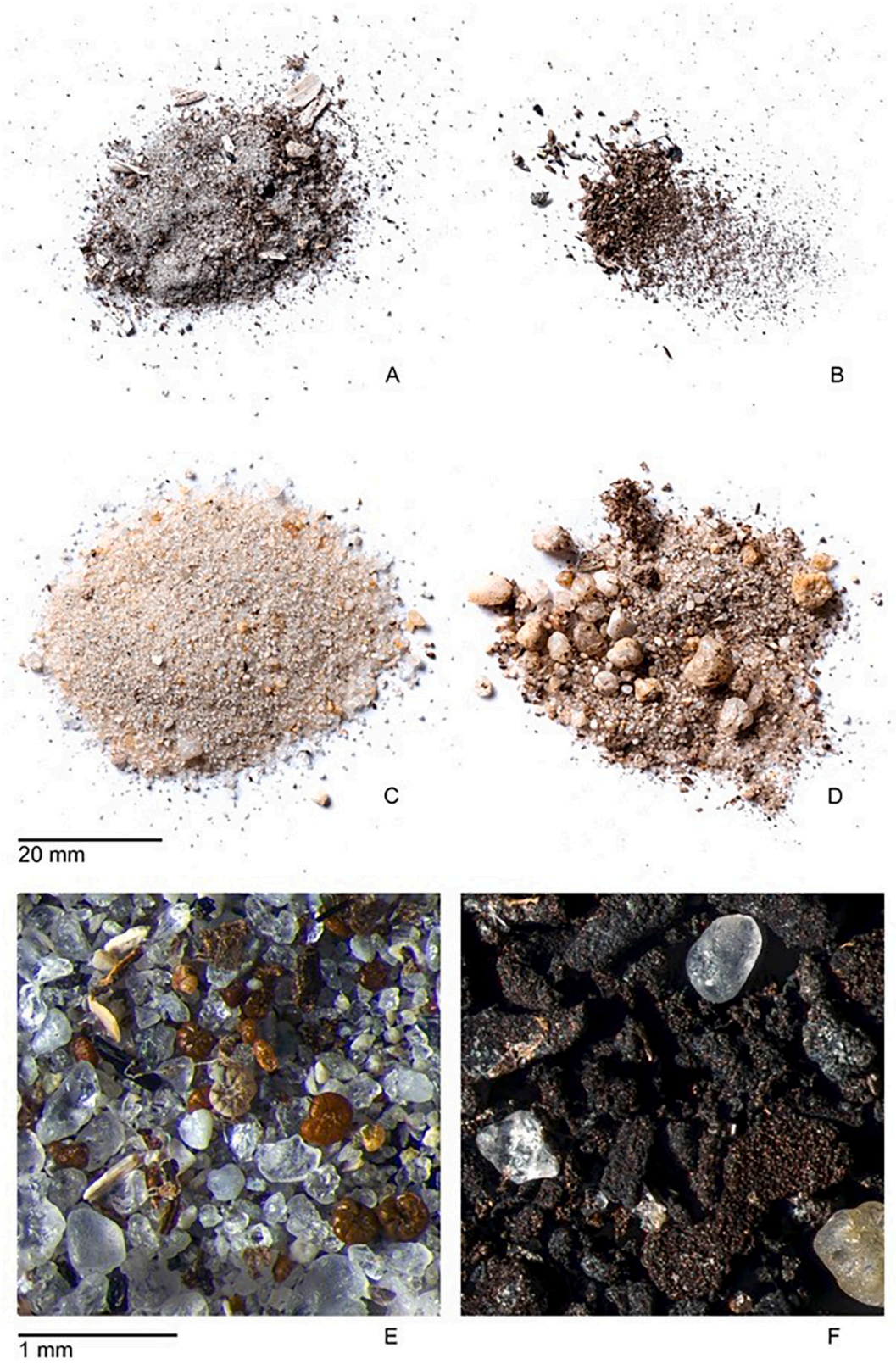

Fig. 7. Total coarse fraction content from: Unit 1, sample Arez3#121146–1148, located at −857 cm MSL (A); Unit 1, transition Unit 1/2, sample Arez3#11966–968, located at −677 cm MSL (B); Unit 3, samples Arez3#2121–123, located at 168 cm MSL (C) and Arez3#1 14–16, located at 275 cm MSL (D). Coarse material detail showing several foraminifera shells, from Unit 1, sample Arez3#121066–1068, located at −777 cm MSL (E); Coarse material detail showing pyritized plant remains, from Sub-Unit 2B, sample Arez3#7566–568, located at −277 cm MSL (F). Photos © José Vicente | Agência Calipo | 2020–2021.

Unit 2 (−677 to 33 cm MSL; 7450 to 4910 cal yrs. B.P.; 5500 to 2960 cal yrs. B.C.) is constituted by mud with the CF always <1%. Total organic matter, C_{org} and N are slightly lower than Unit 1 and vary between 9.8 and 6.2%, 2.1 and 0.3% and 0.17 and 0.06%, respectively, with an upward decreasing tendency (Fig. 6). Taking into consideration in-depth changes in MS, $\delta^{13}C$ and $\delta^{15}N$, three Sub-Units were defined. **Sub-Unit 2A** (−677 and − 390 cm MSL; 7450 to 7040 cal yrs. B.P.; 5500 to 5090 cal yrs. B.C.) has a low MS response, $\delta^{13}C$ is quite constant with mean values of −25‰ and $\delta^{15}N$ has mean values of 4.1% (Fig. 6). The CF is essentially composed by quartz, with the top samples (above −440 cm MSL) mostly composed by pyritized macro plant remains. Pyrite was identified in this Sub-unit, more frequent at the base. In the base of this Sub-unit, foraminiferal assemblage density yielded a Nf/g from 44 to 51 and a H(s) of 1.22 and 1.24. Similarly to Unit 1, it is dominated by *Haynesina germanica* (48 to 49%), *Ammonia tepida* (16 to 19%) and *E. gunteri/oceanensis* (17 to 22%) and followed by the minor *Anomalinoides* cf. *globosus* (6 to 7%). Juvenile specimens of planktonic and marine benthic foraminifera (e.g. *Bolivina* spp., *Fissurina* spp.) are also present. **Sub-Unit 2B** (−390 to −107 cm MSL; 7040 to 6530 cal yrs. B.P.; 5090 to 4580 cal yrs. B.C.) is characterised by a higher frequency in the MS peaks, the $\delta^{13}C$ decreases upwards to lower values of −26‰, while $\delta^{15}N$ has mean values of 4.2% like the Sub-Unit below (Fig. 6). The Sub-Unit's CF is similar to the top samples of Sub-Unit 2A, essentially comprising pyritized macro plant remains with occasional pyrite agglomerates (Fig. 7F). **Sub-Unit 2C** (−107 to 33 cm MSL; 6530 to 4910 cal yrs. B.P.; 4580 to 2960 cal yrs. B.C.) is characterised essentially by changes in the $\delta^{13}C$ and $\delta^{15}N$ values. $\delta^{13}C$ reaches the highest value of −22‰ of the entire sedimentary column at −47 cm MSL. $\delta^{15}N$ has several negative peaks with values <1‰ (Fig. 6). The transition between Unit 2 and Unit 3 is marked by peaks in the organic materials (OM, C_{org} and N) that reach maximum values of 11, 4.2 and 0.3%, respectively at 53 cm MSL (Fig. 6). The CF is composed by Fe concretions (more abundant in the base of the Sub-unit) and quartz grains with Fe coating (more abundant at the top).

Unit 3 (33 to 290 cm MSL; 4910 cal yrs. B.P. to present; 2960 cal yrs. B.C. to present) is essentially characterised as slightly sandy mud and sandy mud, with muddy sand intercalations at 167 cm and between 245 and 250 cm MSL where the CF yielded >60% (Fig. 6). The coarse material is mostly composed by quartz grains, some exhibiting Fe coating and Fe concretions (Fig. 7C and D). The sample collected at 275 cm MSL differs from the other samples, given that is essentially composed of very heterometric quartz grains. Between the base of the Unit (33 cm MSL) and 53 cm MSL, $\delta^{13}C$ values have minimum values of −27‰, the lowest of the sequence (Fig. 6), increasing after to mean values of −26‰. The top 50 cm exhibit high mean $\delta^{13}C$ values of 23‰, decreasing in the very top to values of −26‰. In Unit 3, very low $\delta^{15}N$ values were also measured at the base and at 168 cm MSL, but between 83 and 163 cm MSL values are high with mean values of 6.5‰. In the top 115 cm, $\delta^{15}N$ values exhibit an increasing tendency, growing from values of 4.7 to values of 6.4‰ (Fig. 6).

4.3. Biomarkers

In total, 30 samples were analysed for *n*-alkane content (C_{12} to C_{32}), all with enough material for *n*-alkane analysis. The concentration of *n*-alkanes ranged between 0.06 and 28.1% of total abundance (with exception of C_{30} that was not identified in sample Arez3#4266–268). In general, short-chain *n*-alkanes are more abundant in samples from all the Units (Fig. 8). Despite scarcer, long-chain *n*-alkanes yielded higher concentrations in samples from Unit 3 (Fig. 8). The *n*-alkane C_{15} is the most abundant in all samples with mean values of 16.3% of total abundance (max = 25.0% of total abundance, Arez3#4356–358, Unit 2C; min = 5.4% of total abundance, Arez3#3236–238, Unit 1), with exception in samples Arez3#3204–206 (most abundant *n*-alkane C_{25};

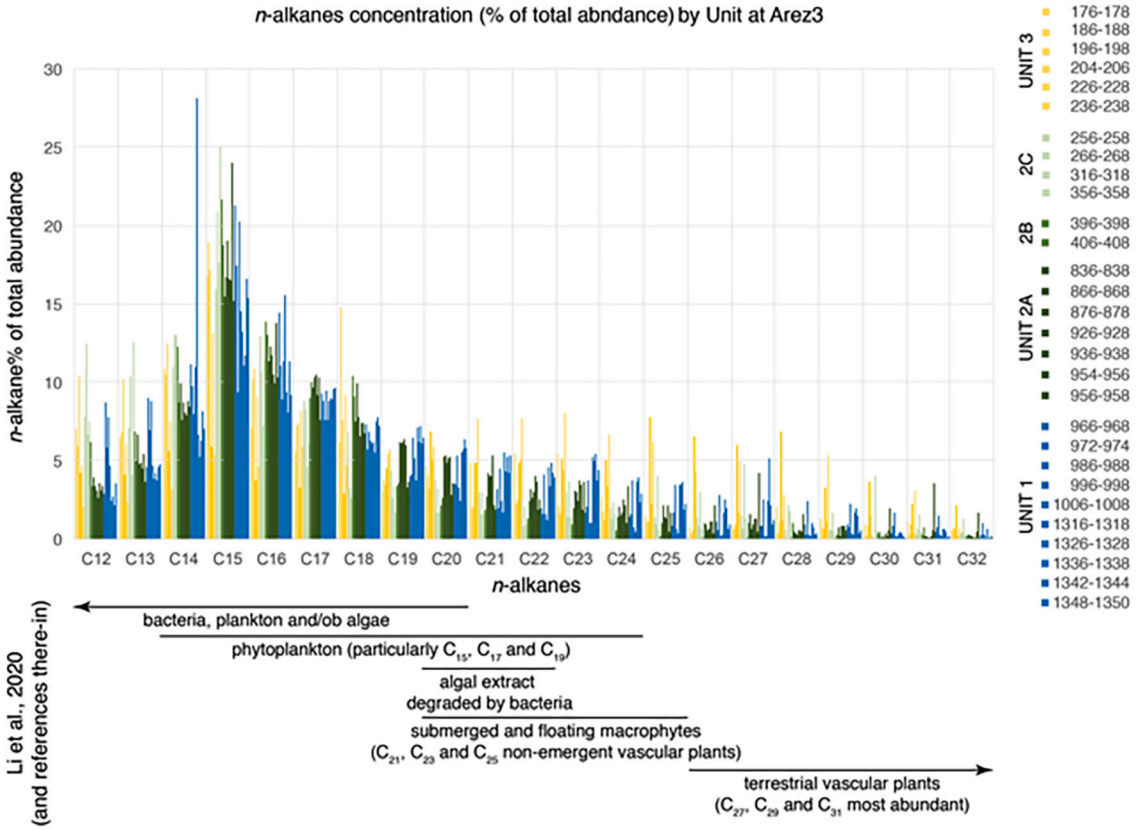

Fig. 8. *n*-alkane % of abundance in Arez3 and organic carbon source information derived from *n*-alkanes retrieved from Li et al. (2020) and references there-in. Colours correspond to the defined Units.

7.8% of total abundance), Arez3#3236–238 (most abundant *n*-alkane C_{23}; 8.1% of total abundance; both from Unit 3) and Arez3#111006–1008 (Unit 1; most abundant *n*-alkane C_{14}; 28.1% of total abundance) (Fig. 8).

The discriminant analysis performed to check the distribution of all *n*-alkanes by the different sedimentary units resulted in an outstanding prediction potential with 100% of the cases grouped in five different clusters corresponding to the Units and Sub-units previously defined (Fig. 9). The result indicates that Units/Sub-units were well separated considering the *n*-alkane concentration and that the source of organic materials differs between each Unit/Sub-unit.

Pristane (Pr) and Phytane (Ph) acyclic isoprenoids were also identified in all samples. Pristane maximum values (4.2% of total abundance) occur at −117 and −577 cm MSL (Sub-unit 2B and 2A) and the minimum value (0.5% of total abundance) was measured at −697 cm MSL (Unit 1). Phytane presents maximum values of 8.8% of total abundance at −667 cm MSL (Sub-unit 2C) and minimum values of 0.3% of total abundance at 85 cm MSL (Unit 3).

In-depth variations of *n*-alkanes proxy ratios are presented in Fig. 10, reflecting differences in the depositional environment and organic matter source (see discussion 5.1). CPI values vary between 1.4 and 0.6, with maximum values at the base of Unit 1 and minimum values at the top of Unit 1. P_{aq} ratio is always higher than 0.6, except on the sample at −667 cm MSL (Sub-unit 2C). TAR is always below 1 with two small peaks in the top of Unit 1 (at −697 and −667 cm MSL; Fig. 10) and two peaks at the base of Unit 3 (at 53 and 85 cm MSL; Fig. 10). TMD varies between 0.9 at 85 cm MSL and 1.5 at −587 cm MSL and Ph/Pr ratio has values lower or equal to 0.8 with some values higher than 0.9 in Sub-unit 2C and Unit 3 (Fig. 10). Ph/C_{17} and Pr/C_{18} present always low values, with maximum mean values of 0.81 and 0.48 represented in Sub-unit 2B (Table 3) pointing to low degradation of *n*-alkanes (e.g. Wang et al., 2008).

4.4. Vegetation

Most of the samples display high values of non-arboreal pollen grains, with exception of the samples collected at −1027 (Unit 1) and −417 cm MSL (Sub-unit 2A; Fig. 11). However, it must be stressed that the main herb represented in this set of samples is Asteraceae Cichorioideae, a taxa with ambiguous significance that may act as indicator of open-ground environments, anthropogenic activities, or marsh flora (Fletcher et al., 2007). Its local character could imply an over-representation of the taxa depending on the scenario, so their values should be taken into careful consideration.

The vegetation in Unit 1 is mainly composed of mixed forests of evergreen and deciduous *Quercus* accompanied by Mediterranean pines (*Pinus halepensis-pinea* type and *Pinus pinaster*) (Fig. 11). Riparian communities are primarily composed by *Alnus* (alder) and they experience a progressive rise from the bottom to the top of the sequence. Unit 1 displays high values of Asteraceae Cichorioideae and the highest percentages of Chenopodiaceae, typical from salt marshes, also appear in this section of the core. The presence of *Isoetes* (freshwater marsh), although permanent and abundant throughout the sequence, seems to be slightly lower in this Unit. It is noteworthy to highlight a slight but progressive increase of heaths since −717 cm MSL (Fig. 12).

Foraminiferal linings (sample − 1027 cm MSL), dinoflagellates (sample − 817 cm MSL), and some specific types of diatoms, such as *Paralia sulcata*, *Triceratium* and *Diploneis* were punctually identified (Fig. 12).

Sub-Unit 2A shares similar characteristics with Unit 1, with a slight decrease of Asteraceae Cichorioideae and the presence of mixed forest, now with a slight rise of Mediterranean trees in their components. *Isoetes* slightly increases, while Chenopodiaceae decreases. Notwithstanding this change, diatoms were also identified in this unit reflecting marine influence.

Sub-Unit 2B is dominated by the presence of Asteraceae Cichorioideae and an abrupt decline of forest and shrublands. *Isoetes* reaches maximum values in this sample (Fig. 12). Some Poaceae bigger than 40 μm were identified in samples from Sub-Unit 2A and 2B (Fig. 11).

In the whole sequence (between −1027 and − 135.5 cm MSL), coprophilous fungi, indicative of anthropogenic activities, and palynomorphs related to erosive processes displayed low values (Figs. 11 and 12).

Concerning the microcharcoal percentages, particles larger than 120 μm and related to local fires, appear in low values, especially in the bottom of the core (Fig. 11). Those particles smaller than 120 μm were present in high values throughout the sequence, with peaks in samples collected at −1027, −817 and − 597 cm MSL, indicating the possible existence of regional fires (Fig. 11).

5. Discussion

5.1. Sources of organic matter

Estuaries are transitional areas between fluvial and marine environments and constitute sediment sinks for material brought downstream by the fluvial network, for material transported landward from the sea (allochthonous material), and for organic material produced in the estuarine basin (authochthonous material) (Schubel, 1982; Meyers, 1994; Khan et al., 2015; Scanes et al., 2019). Organic proxies, such as

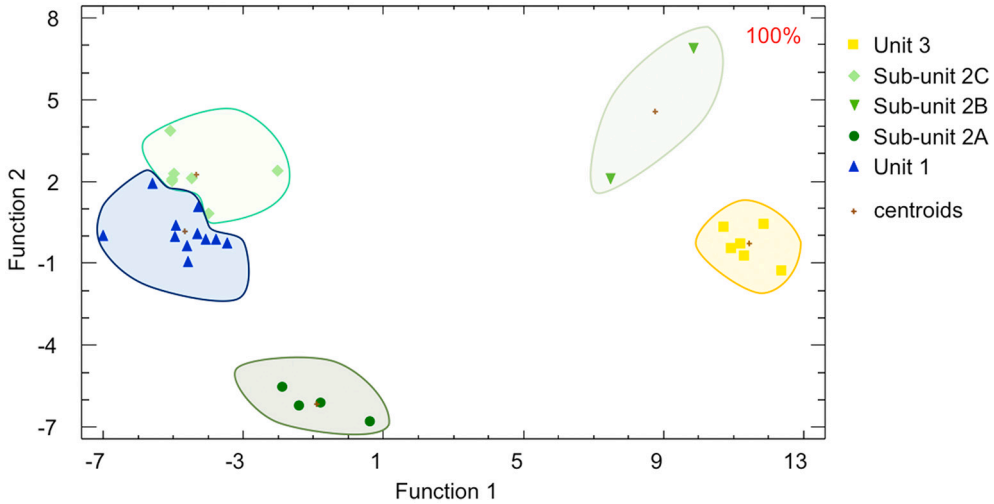

Fig. 9. Discriminant analysis using the *n*-alkanes series (C_{12} to C_{32} alkanes) as variables and the sedimentary units (Units 3, 2C, 2B, 2A, 1) as classification factor.

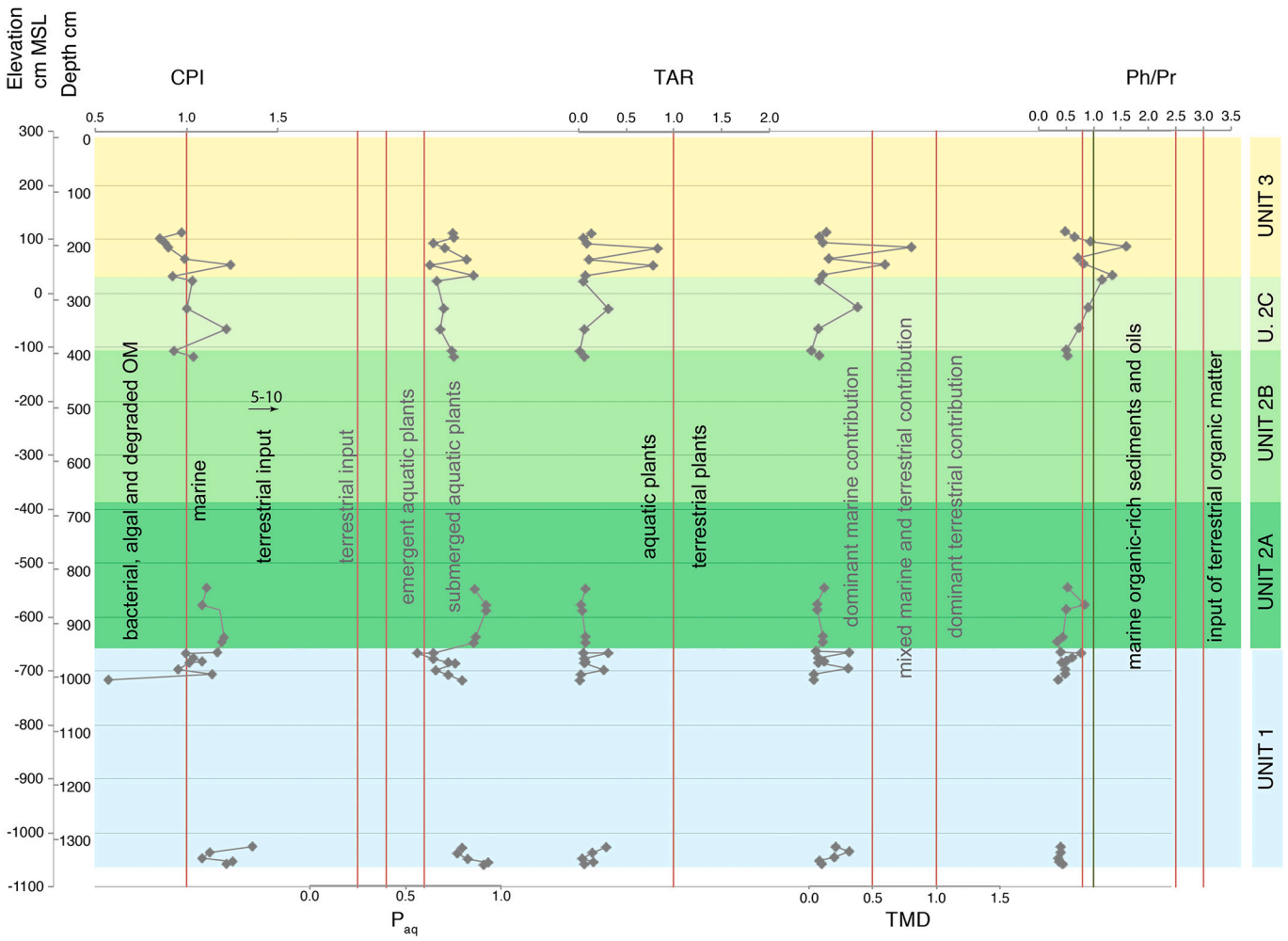

Fig. 10. In-depth variation of n-alkane and acyclic isoprenoid ratios against elevation cm MSL and depth cm: CPI, P_{aq}, TAR, TMD and Ph/Pr. Diagnostic values and references described in Table 3. Green vertical line in Ph/Pr indicates anoxic (<1) / oxic (>1) environments (e.g. Powell, 1988; Hughes et al., 1995). (For interpretation of the references to colour in this figure legend, the reader is referred to the web version of this article.)

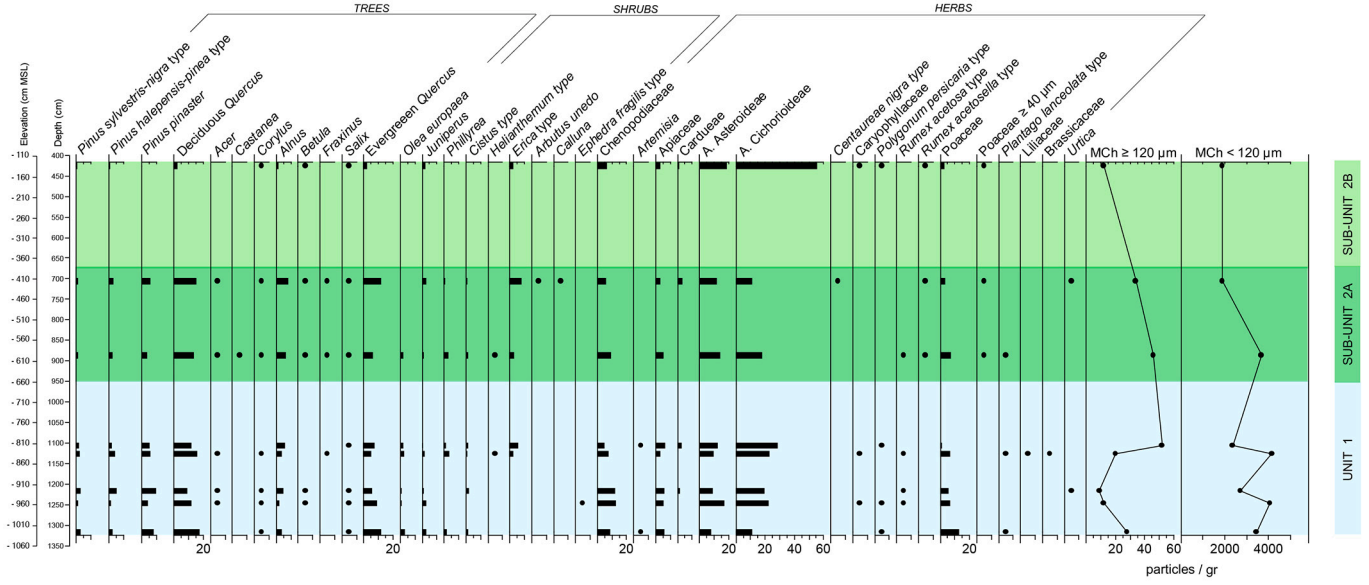

Fig. 11. Percentage pollen diagram for trees, shrubs, and herbs. Black dots represent percentages below 3%. Microcharcoal particles (MCh) are expressed in particles /gr of dry sediment (concentrations).

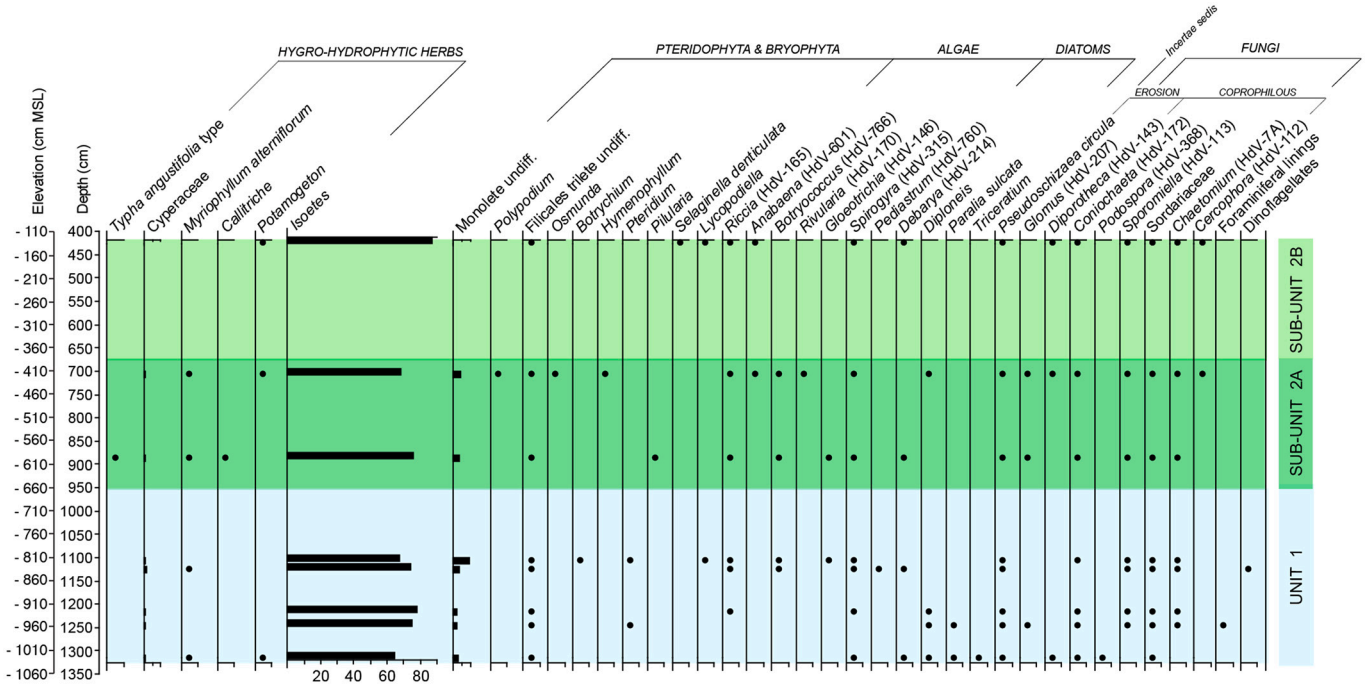

Fig. 12. Percentage pollen diagram for aquatic herbs, ferns and mosses, diatoms, and Non-Pollen Palynomorphs (NPPs). Black dots represent percentages below 3%.

$\delta^{13}C$, $\delta^{15}N$ and C/N are widely used to distinguish between the organic matter sources, helping to characterise past environments (Wilson et al., 2005; Lamb et al., 2006; Khan et al., 2015). In addition, lipid biomarkers and indices are pertinent indicators of palaeoenvironmental conditions and organic matter source (Meyers, 2003; Ouyang et al., 2015; Li et al., 2020).

In Arez, while $\delta^{15}N$ only exhibits significant changes in the top unit (Sub-unit 2C and Unit 3), $\delta^{13}C$ seems to reflect different organic sources as a function of depth (Fig. 6). Fig. 13 shows data from Arez3 and Arapouco (sediment core collected in the main Sado channel, near Arez3; Fig. 1; first published in Costa et al., 2019) plotted in a chart draw by Lamb et al. (2006) and updated by Khan et al. (2015). Both publications compile information from several studies that investigated the source of organic matter in intertidal wetland areas using $\delta^{13}C$ and C/N values measured in sediments. According to this chart, Unit 1, characterised by strong variations in the $\delta^{13}C$ values, seems to reflect constant changes in the source of organic materials from marine (higher values; −23‰; Marine Dissolved Organic Carbon (DOC)) and freshwater/terrestrial environments (lower values; −26‰; Freshwater DOC and Macroalgae/C3 Terrestrial plants; Figs. 6 and 12) (Lamb et al., 2006 and references there-in). Values are quite similar to the ones determined for Units 2 to 4 from Arapouco (Fig. 13). In addition, *n*-alkanes total abundance exhibits higher values in short chain *n*-alkanes C_{12} to C_{19}, pointing to the existence of an aquatic environment, with a gradual

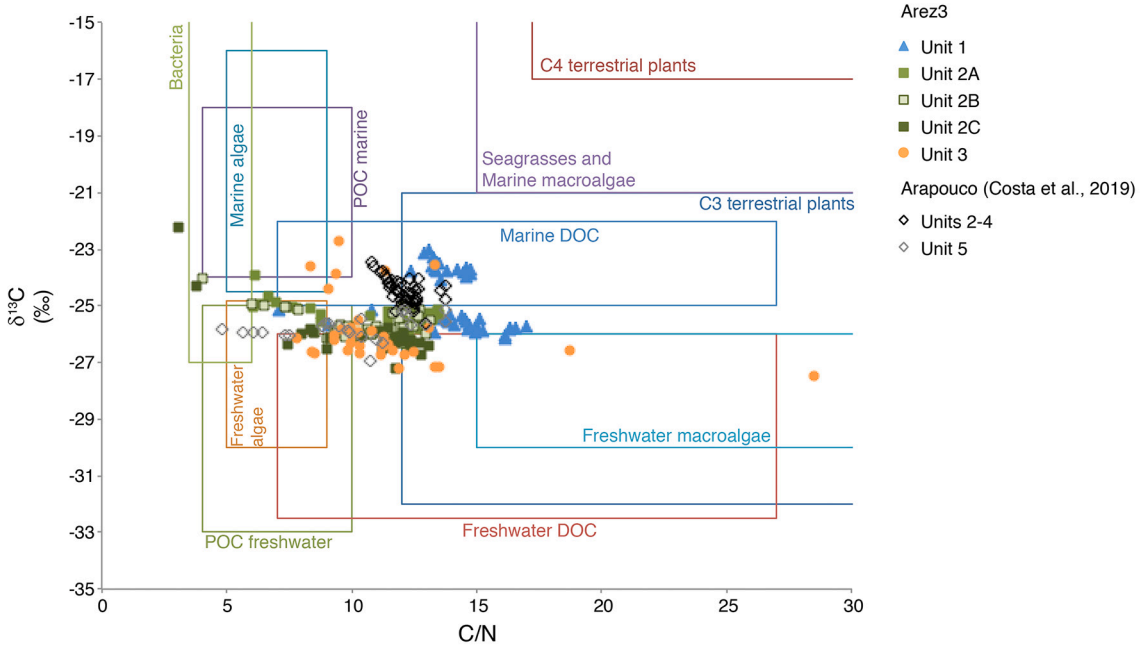

Fig. 13. C/N vs. $\delta^{13}C$ results from Arez 3 and Arapouco (Costa et al., 2019) plotted in the adapted graph from Lamb et al.'s (2006), updated by Khan et al. (2015).

decreasing tendency to the top if mid- and long-chain *n*-alkanes are considered (Fig. 8). Maximum values in C_{15} are usually related to phytoplankton (Fig. 8; e.g. Li et al., 2020). Carbon preference index (CPI; values near 1 and slightly higher) and TMD (values lower than 0.5) ratios seem to reflect a dominance of marine OM in Unit 1 with occasional terrestrial inputs (Fig. 10). Ph/Pr ratios values in Unit 1 also fall within the marine organic-rich sediments values deposited in an anoxic environment (Powell, 1988; Hughes et al., 1995; Meyers, 2003), i.e., presenting less favorable environmental conditions for the degradation of organic matter (Meyers, 2003). Anoxic conditions are also attested by the presence of pyrite agglomerates and the precipitation of pyrite on the macro-plant remains. Higher abundance of mid-chain *n*-alkane (C_{21} to C_{25}), which are usually attributed to submerged and floating aquatic plants including marine macrophytes (Sikes et al., 2009), than long-chain *n*-alkanes (Fig. 8) and a P_{aq} value ca. 0.9 in the base of Unit 1 and Sub-unit 2A (Fig. 10; Mean values of 0.8; Table 3; Ficken et al., 2000; Sikes et al., 2009) point to the importance of aquatic plants contributing to the OM content during this period.

In Units 2 and 3, the $\delta^{13}C$ exhibits an upward decreasing tendency (from −25‰ to −27‰; Fig. 6), reflecting an increase in the contribution of OM from terrestrial plants and freshwater phytoplankton (Freshwater DOC, Particulate Organic Carbon (POC) and algae) to the sediment through time (Fig. 13). Again, values are within the range of the $\delta^{13}C$ determined for Unit 5 in Arapouco (Fig. 13), corresponding to the aggradation of the alluvial plain (Costa et al., 2019).

The relative total abundance of long-chain *n*-alkanes, particularly in Unit 3, also points to higher inputs of terrestrial organic materials (Fig. 8).

In Sub-unit 2C and Unit 3, $\delta^{13}C$ exhibits sharp peaks with values $\geq$ −24‰ (Fig. 6). These values can result from higher marine influence, with contributions from marine algae and marine POC, from the presence of bacteria, at least considering the lower values from Sub-Unit 2C (Fig. 13) or from runoff inputs enriched in N-fertilisers (Bogaard et al., 2013).

$\delta^{15}N$ also exhibits several negative peaks in Sub-unit 2C and Unit 3, reaching values of 0‰ (Fig. 6). Changes in $\delta^{15}N$ values are related with nitrogen cycle processes and/or with N source (Yamamuro et al., 2003; Torres et al., 2012; Golubkov et al., 2020). At present, high $\delta^{15}N$ isotopic values in aquatic environments are usually related to polluted areas due to e.g. sewage inputs and fertilisers runoff and are frequently used as a tracer for human activities (Meyers, 2003; Yamamuro et al., 2003; Lepoint et al., 2004; Laussaque et al., 2010; Connolly et al., 2013). Recent studies showed that depletion in ^{15}N (0‰ or lower $\delta^{15}N$ values) could also be related to ammonium peaks in highly polluted aquatic systems (e.g. Kopprio et al., 2018). In pristine aquatic systems, $\delta^{15}N$ isotopic values are usually lower than in systems with anthropic influence, and most are related to the source of organic matter (Meyers, 2003), and the microbial processes of nitrification, denitrification, and N-fixation (Scanes et al., 2019). In general, $\delta^{15}N$ isotopic ratio increases from oligotrophic to eutrophic systems, but decreases in hyper-euthrophic and anoxic conditions due to the presence of cyanobacteria (Meyers, 2003; Gu, 2009; Golubkov et al., 2020). In diverse aquatic systems $\delta^{15}N$ values ~0‰ were related to N-fixation processes and the dominance of N-fixing cyanobacteria in the phytoplankton community (Yamamuro et al., 2003; Torres et al., 2012; Bardhan et al., 2017).

Sub-Unit 2C deposited between ca. 6530 to 4910 cal yrs. B.P. (i.e. 5500 to 2960 cal yrs. B.C.), so the incorporation of ^{15}N enriched OM from sewage or N-enriched fertilisers can be ruled out, with the negative shift of $\delta^{15}N$ to values ~0‰ most probably explained by hyper-eutrophication and by cyanobacteria bloom episodes. Similarly, in Unit 3, deposited in the last ca. 5000 years, the negative shifts in $\delta^{15}N$ values that occurred at ca. 4650 cal BP (ca. 2700 cal yrs. B.C.) and ca. 3525 cal yrs. B.P. (ca. 1575 cal yrs. B.C.) appear to be more related to bacterial activity. Frequent CPI values lower than 1 in Sub-unit 2C and Unit 3 are also indicative of microorganisms, bacterial communities, and degraded OM (Fig. 10; e.g. Bray and Evans, 1961), and Ph/Pr changes between values > and <1 (Table 3 and Fig. 10) point to the alternation between oxic and anoxic environments suitable for the degradation of organic matter and eutrophication events.

Only the more recent $\delta^{15}N$ negative peak (ca. 790 cal yrs. B.P.; 1160 cal yrs. A.D.; Fig. 6) can be associated with anthropic activities. Indeed, between the top-most negative $\delta^{15}N$ shifts, $\delta^{15}N$ values increase to values higher than 6‰ (Fig. 6) that can be related with organic matter derived from algae (+8.5‰; Meyers, 2003), but also from heavy nitrate fertilisers and human sewage (Teranes and Bernasconi, 2000). Unit 3 deposited above present-day MSL, and despite the possibility of being flooded during high tides, the presence of marine algae influencing $\delta^{15}N$ is not plausible, given that in-depth $\delta^{15}N$ are lower even during higher marine influence episodes (Unit 1; Fig. 6). The alluvial plain of Carrasqueira stream, where Arez3 was collected, is nowadays used for agriculture practices, particularly rice production, as it happens in the Sado channel alluvial area (Costa et al., 2019; 2021). The $\delta^{13}C$ higher values measured in the top of Unit 3 can also be related to the input of N-fertilisers given that changes in the $\delta^{13}C$ values are known to occur by the input of mineral N-fertilisers (e.g. Bogaard et al., 2013). Finally, the increase of $\delta^{13}C$ values in the top sediments from the Sado alluvial plain are related to anthropic activities, as recently described by Costa et al. (2021).

5.2. Holocene environmental evolution

During the Early Holocene and the beginning of the Middle Holocene, the MSL was rising at a rate of 0.81 ± 0.07 cm yr^{-1} in the SW Atlantic Portuguese margin (García-Artola et al., 2018), which is higher than the sedimentation rate obtained in Arez3 (between 0.22 and 0.64 cm yr^{-1}; Fig. 4). This circumstance allowed for the flooding of the incised Carrasqueira valley, and certainly other similar tributaries of the Sado; the rise in the MSL is therefore the main factor responsible for the extensive flooding of the area. Similarly, the sedimentation rate only surpassed the MSL rise rate between 7120 and 6800 cal yrs. B.P. (i.e. 5170 and 4850 cal yrs. B.C.; Fig. 4), after the deceleration of the sea-level rise (García-Artola et al., 2018), achieving high values of 1.2 cm yr^{-1} (Fig. 4) and promoting the vertical accretion of the valley bottom and estuarine basin from that date onwards. The Carrasqueira is a high-gradient stream with torrential hydraulic regime, and thus an important contributor of sediments to the lower section of the valley that has certainly played a role in the high sedimentation rate estimated for the area during the beginning of the Middle Holocene.

According to the age-model, the sedimentary infilling of the Sado estuary seems to follow the same depositional pattern of other SW Iberian estuaries (Dabrio et al., 2000; Boski et al., 2002, 2008; Lario et al., 2002; Vis et al., 2008; Camacho et al., 2016) despite the higher mean sedimentation rates determined in all the cores collected in the Sado valley (this work and Costa et al., 2021), thus reflecting the strong Mediterranean character of the Sado basin.

The multiproxy analyses performed in the Arez3 sedimentary sequence allowed to identify marine influence between ca. 8850 and 7040 cal BP (ca. 6900 and 5050 cal BP). The results revealed an estuarine environment similar to the present-day Sado estuarine basin, suitable for the development of shellfish banks. This fact is evidenced by the presence of foraminifera in Unit 1 and Sub-unit 2A that usually are not preserved in Sado sediments due to under saturated $CaCO_3$ conditions. The under saturated $CaCO_3$ environment is also corroborated by the punctual appearance of foraminifera linings as identified in other Atlantic estuaries (Moreno et al., 2007; Valente et al., 2009). However, foraminiferal assemblages dominated by the species *Haynesina germanica*, *Ammonia tepida* and *E. gunteri/oceanensis* are also recorded, with a low value of foraminiferal density and diversity index that indicates a brackish environment. Such conditions and the presence of juveniles from planktonic and marine benthic foraminifera (e.g. *Bolivina* spp., *Fissurina* spp.) clearly indicate that a marine influence was present by that time. Such assemblage is today found in the Sado estuary in subtidal

and tidal flat environments (Fatela et al., 2009). Additionally, the absence of agglutinated species such as *Jadammina macrescens* and *Trochamina inflata*, dominant on marsh zones, and the presence of exotic juvenile marine specimens, dragged upstream by tidal currents, reinforces the notion that this palaeoenvironment was a low riverbank, under permanent submersion. The presence of Chenopodiaceae together with the occasional occurrence of dinoflagellates, and some specific types of diatoms (e.g. *P. sulcata*, *Triceratium*, and *Diploneis*) identified during pollen analyses also point to the existence of a brackish environment. In addition, marine and brackish diatoms assemblages characterised by epipsammic diatoms, with *Opephora mutabilis* being the most frequent taxon, and sponge spicules were also found at the base of Arez1 (between −775 and − 798 cm MSL; dated to ca. 8500 cal yrs. B.P.; Costa et al., 2020).

The freshwater environments slightly increase in relation to salt marsh communities between 7450 and 7040 cal yrs. B.P. (5500 to 5090 cal yrs. B.C.) as evidenced by a decrease in Chenopodiaceae and a slightly decline in Asteraceae Cichorioideae, while *Isoetes* slightly increases (Figs. 13). In addition, C/N and $\delta^{13}C$ of Sub-unit 2A point, to some extent, to the presence of freshwater POC and freshwater algae, confirming the increased influence of freshwater environments (Fig. 13).

Towards the top of the sequence (Sub-Units 2B and 2C; 7040 to 4910 cal yrs. B.P.; 5090 to 2960 cal yrs. B.C.), the increase in the contribution of OM from terrestrial plants and freshwater phytoplankton (Fig. 13) suggest higher influence of the river(s) in the area and the expansion of freshwater wetlands in detriment of brackish environments. This is also corroborated by the decrease of Chenopodiaceae and the high values of *Isoestes*. This is compatible with a scenario in which the rate of MSL rise decreases (García-Artola et al., 2018) whilst sedimentation rates increase (Fig. 4), promoting the fast silting-up of the valley.

In terms of vegetation, an abrupt decline of the forest and shrublands was identified in Sub-unit 2B (Fig. 11), suggesting an open ground environment, maybe related to the increase of human pressure. These results seem to relate to the generalised forest decline identified in diverse sequences of SW Iberia from 7000 cal yrs. B.P. onwards (Cambourieu-Nebout et al., 2009; Chabaud et al., 2015; Fletcher et al., 2007; Fletcher and Sánchez Goñi, 2008; Gomes et al., 2020; Vis et al., 2010).

The presence of some Poaceae grains ≥40 μm in Sub-unit 2B can be associated to the domestication of wild grasses resulting from arable activity, but large pollen grains of Poaceae may also be related to wetland wild grasses (Tweddle et al., 2005).

Unit 3, deposited above present-day MSL under a low sedimentation rate (excepting the top 180 cm; Fig. 4) and receiving material mostly sourced in freshwater environments (see discussion 5.1), corresponds to the aggradation of the alluvial plain, with the sedimentation rate being dependent on the (low) accumulation space and river dynamics (floods).

Eutrophication events with the development of bacterial communities seem to have occurred sporadically since ca. 6530 cal yrs. B.P. (Sub-unit 2C and Unit 3; see discussion 5.1) pointing to the development of backswamp environments in the Carrasqueira valley, since the Middle Holocene. Also, ca. 6500 cal yrs. B.P. the formation of the Tróia sand spit starts, followed by its progradation northwards (Costas et al., 2015), creating the present-day bar-built estuarine area and limiting the exchanges between the estuary and the open sea. By then, and mostly on account of the deceleration of sea-level rise, the nearby coastal depressions of e.g. Santo André and Melides became isolated from the sea by the formation of sandy barriers, forming stable coastal lagoons that remained as such until the end of the 3rd millennium BP (Freitas et al., 2003; Cabral et al., 2006; Laermanns et al., 2021).

Recently, the effects of anthropic activities also led to changes in the sediment organic chemistry.

Despite the fast silting-up and the development of freshwater environments at the Carrasqueira valley since ca. 7040 cal yrs. B.P. (Sub-Unit 2B), brackish environments and marine influence were present in Arapouco (Sado channel; Fig. 1) at least until 3240 cal yrs. B.P., after which the aggradation of the alluvial plain took place (Costa et al., 2019).

5.3. Sado late Mesolithic environments

Late Mesolithic occupation in the Sado surrounding areas took place between 8400 and 7000 cal yrs. B.P. (Arias et al., 2017; Peyroteo-Stjerna, 2020) and is contemporaneous of the deposition of Unit 1 and Sub-unit 2A (8850 to 7040 cal yrs. B.P.; Fig. 4; Table 2). During this time span, MSL was rising at a high rate in the SW Atlantic margin (e.g. García-Artola et al., 2018), allowing for the flooding of the incised Sado and Carrasqueira valleys, and presumably other tributaries of the Sado. By then, the estuary was still an open bay and late Mesolithic sites were located between ca. 25 km (Arapouco, at the proximity of the Carrasqueira stream) and 45 km (Laxique) from the open sea.

At ca. 8400 cal yrs. B.P. the MSL was ca. -970 cm MSL and rose to −240 cm MSL at ca. 7500 cal yrs. B.P. (Fig. 4) while sediments corresponding to this time interval can be found approximately between −1060 and − 390 cm MSL (Unit 1 and Sub-unit 2A), revealing an extensive drowned area during the late Mesolithic occupation. This fact is consistent with the existence of an aquatic environment as revealed by the contribution of aquatic plants to the OM source (see discussion 5.1). The MSL rose to −160 cm MSL at ca. 6900 cal yrs. B.P., but contemporary sediments occur at −10 cm MSL thus reflecting a change in the environmental conditions with intertidal areas occupying previous drowned areas.

During the late Mesolithic occupation, the high intertidal areas of the Carrasqueira stream (developing in the shallow margins; Fig. 3) and other similar valleys (see discussion 5.3) were certainly colonised by marsh communities, as reflected by the organic chemistry results (Fig. 13) and the palynological content of Arez3, with high percentages of Chenopodiaceae (salt marsh) and the presence of *Isoetes* (freshwater marsh; Figs. 13). A higher marine influence was detected until ca. 7500 cal yrs. B.P. (5550 cal yrs. B.C.), when freshwater environments started to increase.

In the emerged landscape, mesophilous trees (mainly deciduous *Quercus*) were more abundant than other arboreal taxa, suggesting mostly the existence of a moist climate during the late Mesolithic occupation. High-mountain pines (*Pinus sylvestris-nigra* type), usually related to continental climate, also occurred but with low representation. Mediterranean pines, such as *P. halepensis-pinea* type and *P. pinaster*, were also represented (Fig. 11), probably distributed across the interdune depressions. In Sub-unit 2A, a slight rise of Mediterranean trees occurred, indicating the presence of temperate elements within the forests.

5.4. Suitable areas for the collection of shellfish during the Mesolithic in the Sado valley

The Alcácer do Sal (palaeo)intertidal area was pointed out as the local used by Mesolithic groups for the collection of shellfish, based on the presence of foraminifera shells and calcareous pebbles among the shell midden content of Poças de São Bento shell midden (Duarte et al., 2019; PSB; Fig. 1).

Presently, despite not being the most abundant species, *S. plana* and *Cerastoderma* still occur in the Sado estuary. *S. plana* is essentially identified in the Alcácer do Sal channel in mud to fine sand sediments with lower salinity contents. Likewise, *Cerastoderma* spp. is identified in the Alcácer do Sal channel, but also in the central estuarine basin, with salinity (values between 17 and 30‰), grain-size (fine sediments), OM content, and water depth (shallower areas) being the most important factors contributing to its distribution (Santos, 2019). Our observations suggest that suitable conditions (i.e. salinity, organic fine sediments and shallow margins) for the occurrence of *S. plana* and *C. edule* were present at the Carrasqueira valley (and presumably in other similar valleys) during the late Mesolithic occupation, allowing its exploitation by the Mesolithic groups over a much wider area than previously thought.

S. plana shell fragments were described in Arez3 sediments, particularly between the base of the core and − 360 cm MSL (Unit 1, Sub-unit 2A and partially Sub-unit 2B), confirming the presence of this species in this area of the Sado valley during the Early-Middle Holocene.

In the wider array of fish identified in Arapouco and Poças de S. Bento, marine/estuarine taxa prevail. The identified taxa (e.g. *Chellon labrosus*, *S. aurata*, *A. regius* and *Dicentrarchus* sp.) still occur in the estuary (Sobral, 1993; Cabral, 1997; Cunha et al., 2014), feeding on various kinds of bottoms. The young form, school and feed chiefly on invertebrates, molluscs, and also on other fishes. Assuming fish behavior has not changed since Mesolithic times, and considering individual size estimates from archaeological bones, one can assume that Mesolithic communities exploited the surrounding environments targeting large schools of young fish (e.g., *A. regius* and *Dicentrarchus* sp.; Gabriel et al., 2012; Gabriel, unpub. data).

Based on a morphological analysis (length and width of the alluvial plain), and on data previously produced for the Sado valley concerning the palaeovalleys depth and morphology (Costa et al., 2020), and also data presented in this work, other tributaries of the Sado upstream Alcácer do Sal - such as the Santa Catarina and Alfebre streams (Fig. 1) - could have had the same suitable environmental conditions for the development of molluscs and thus conditions for the exploitation of these resources by Mesolithic people. A study performed at Vale dos Açudes located ca. 6.5 km upstream Carrasqueira (Fig. 1; Costa et al., 2020), revealed a very shallow palaeovalley without marine influence. Similarly, brackish conditions in shallow tributaries of the Sado located upstream Vale dos Açudes should be absent. The Algalé (or Alcaçovas) stream is longer and has a larger alluvial plain pointing to a deeper palaeovalley, but the scarcity of data in this section of the Sado valley hamper a full characterization of its environmental conditions.

The morphology of the Sado channel as characterised by ERT data (Costa et al., 2020) seem to exhibit deep steep margins, presenting less suitable conditions for the development of extensive marshes and/or tidal flats. However, less incised upstream areas of the Sado river would certainly have offered conditions for the development of intertidal environments. Notwithstanding this condition, the maximum limit of marine inundation during the Early and Middle Holocene in the Sado channel is still unknown. Recent work published by Costa et al. (2021) attest the occurrence of estuarine conditions during the Mid-Late Holocene transition (between 4350 and 4000 cal yrs. B.P.) in a sediment core, at Laxique, collected ca. 65 km upstream the present-day estuary inlet. At this location, the sedimentation is mostly influenced by low river discharges associated with a dry climate pattern rather than MSL oscillations. Nevertheless, studies of deep sediment cores covering the Holocene sedimentary succession are necessary to fully evaluate the marine inundation prior to 4350 cal yrs. B.P. at the upstream limits of the Sado estuary.

6. Conclusions

The multiproxy analysis of the 13.5 m Arez3 sedimentary sequence recovered from the Carrasqueira stream, a tributary of the Sado valley located at ca. 52 km upstream the present-day estuarine inlet, revealed to be a critical source of information concerning environmental conditions of the Sado valley during the late Mesolithic occupation. Estuarine conditions, similar to the present-day central estuarine basin, existed at the Carrasqueira valley at least between ca. 8850 and 7450 cal yrs. B.P. (6900 and 5500 cal yrs. B.C.) and prevailed, despite the higher freshwater influence, until ca. 7040 cal yrs. B.P. (5090 cal yrs. B.C.), i.e. during the occupation of the valley by the late Mesolithic communities. Such conditions allowed for the development of mollusc banks, such as *S. plana* and *C. edule*, which were exploited by these hunter-gather communities in the intertidal areas (salt marshes and tidal flats) of the valley.

Since ca. 7040 cal BP the sedimentation rates surpassed the sea-level rise rates, leading to the silting-up of the valley and allowing for the progressive progradation of freshwater environments downstream. Other valleys with extension and valley morphology similar to the Carrasqueira valley, should have exhibited similar estuarine conditions during the late Mesolithic.

Author contributions

All authors have made substantial contributions to this manuscript. AMC, MCF, PA and MD conceived the study. AMC made sedimentological analyses and wrote the manuscript. AMC and MCF made the discussion, interpretation and integration of the results. MCF made morphoscopy of the coarse fraction. MAJ-G, NTJ-M and CBD made the biomarkers analyses. CV-P and KR made the palynological analyses. KR was responsible for core collection. FF was responsible for the foraminiferal assemblages identification. ACA added information concerning the late Mesolithic shell middens. SG added information concerning aquatic resources (fish) in the Sado estuary. ML helped in the diatom interpretations and is responsible for organic chemistry analyses. All authors commented and contributed to improve the manuscript.

Funding

This work was done with-in the PhD grant funded by FCT (SFRH/BD/110270/2015) attributed to Ana Maria Costa between 2016 and 2019 and took advantage of financial support from the projects SimTIC (HAR2017-82557-P) financed by the Spanish Ministry of Science and Innovation, Back to Sado (PTDC/HIS-ARQ/121592/2010) funded by FCT. The authors would also like to acknowledge the support of the Instituto Dom Luiz - IDL (UIDB/50019/2020).

Data Availability

The data and analysis scripts can be found at https://doi.org/10.17632/f48y6h6x6r

Declaration of Competing Interest

The authors declare that they have no known competing financial interests or personal relationships that could have appeared to influence the work reported in this paper.

Acknowledgements

The authors would like to acknowledge Ana Filipa Fernandes, Barbara Wagner, Hannes Laermanns, Lukas Kienzler and Sebastian Frank who helped on the core collection. The authors are also thankful to Vera Lopes and Ricardo Santos who helped in the total organic matter analyses, to José Vicente for the photographs and to Mário Cachão for the observation of smear slides and the identification of sponge spicules and diatoms in Arez1, in barren nannoplankton sediment. Ricardo Ramalho revised the English.

References

Antunes, M.T., Pais, J., Lopes, J.C., 1983. Carta Geológica de Portugal 1:50000 Folha 39C Alcácer do Sal. Serviços Geológicos de Portugal, Direcção Geral de Geologia e Minas.

Antunes, M., Pais, J., Gonçalves, F., Oliveira, J., Peleja, A.F., Barroso, J.P., Romão, J.A., Lopes, J.C., Casimiro, J., 1991. Carta Geológica de Portugal 1:50000 Folha 39-D Torrão. Serviços Geológicos de Portugal, Direcção Geral de Geologia e Minas.

Araújo, A.C., 1997. A indústria lítica do concheiro de Poças de S. Bento (vale do Sado) no seu contexto regional. O Arqueólogo Português 13/15, série IV, pp. 87–159.

Araújo, A.C., 2015. A few steps backwards…, in: Search of the origins of the late Mesolithic. In: Bicho, N.F., Detry, C., Price, D., Cunha, E. (Eds.), Muge 150th: The 150th Anniversary of the Discovery of Mesolithic Shellmiddens, vol. 2. Cambridge Scholars Publishing, pp. 1–15.

Arias, P., Diniz, M.T., Araújo, A.C., Armendariz, Á., Teira, L.C., 2015. At the edge of the marshes: New approaches to the Sado valley Mesolithic (southern Portugal). In: Bicho, N.F., Detry, C., Price, T.D., Cunha, E. (Eds.), Muge 150th: The 150th

Anniversary of the Discovery of Mesolithic Shellmiddens, Vol. 1. Cambridge Scholars Publishing, pp. 301–319.
Arias, P., Diniz, M.T., Cubas, M., Duarte, C., Iriarte, E., Salzmann, C., Teichner, F., Teira, L.C., 2017. Looking for the traces of the last hunter-gatherers: Geophysical survey in the Mesolithic shell middens of the Sado valley (southern Portugal). Quat. Int. 435 (B), 61–70. https://doi.org/10.1016/j.quaint.2016.02.016.
Arnaud, J.M., 1987. Os concheiros dos vales do Tejo e Sado: semelhanças e diferenças. Arqueologia 15, 53–63.
Arnaud, J.M., 1989. The Mesolithic communities of the Sado valley (Portugal) in their ecological setting. In: Bonsall, C. (Ed.), The Mesolithic in Europe, Papers Presented at the III International Symposium. John Donald, Edinburgh, pp. 614–631.
Arnaud, J.M., 2000. Os concheiros mesolíticos do vale do Sado e a exploração dos recursos estuarinos (nos tempos pré-históricos e na actualidade). Trabalhos Arqueol. 14, 21–43.
Bardhan, P., Naqvi, S.W.A., Karapurkar, S.G., Shenoy, D.M., Shenoy, D.M., Kurian, S., Naik, H., 2017. Isotopic composition of nitrate and particulate organic matter in a pristine dam reservoir of westen India: implications for biogeochemical processes. Biogeoscences 14, 767–779. https://doi.org/10.5194/bg-14-767-2017.
Bettencourt, A., Ramos, L., 2003. Estuários Portugueses. Lisboa: Direcção de Serviços do Planeamento, Instituto da Água, Ministério das Cidades, Ordenamento do Território e Ambiente.
Bicho, N., Cascalheira, J., Marreiros, J., Gonçalves, C., Pereira, T., Dias, R., 2013. Chronology of the Mesolithic occupation of the Muge valley, Central Portugal: the case of Cabeço da Amoreira. Quat. Int. 308-309, 130–139. https://doi.org/10.1016/j.quaint.2012.07.223.
Blaauw, M., 2010. Methods and code for 'classical' age-modelling of radiocarbon sequences. Quat. Geochronol. 5 (5), 512–518. https://doi.org/10.1016/j.quageo.2010.01.002.
Bogaard, A., Fraser, R., Heaton, T.H.E., Wallace, M., Vaiglova, P., Charles, M., Jones, G., Evershed, R.P., Styring, A.K., Andersen, N.H., Arbogast, R.-M., Bartosiewicz, L., Gardeisen, A., Kanstrup, M., Maier, U., Marinova, E., Ninov, L., Shäfer, M., Stephan, E., 2013. Crop manuring and intensive land management by Europe's first farmers. Proc. Nat. Acad. Sci. United States Am. 110 (31), 12589–12594. https://doi.org/10.1073/pnas.13059181110.
Boski, T., Moura, D., Veiga-Pires, C., Camacho, S., Duarte, D., Scott, D.B., Fernandes, S. G., 2002. Postglacial Sea level rise and sedimentary response in the Guadiana Estuary, Portugal/Spain border. Sediment. Geol. 150, 103–122. https://doi.org/10.1016/S0037-0738(01)00270-6.
Boski, T., Camacho, S., Moura, D., Fletcher, W.J., Wilamowski, A., Veiga-Pires, C.C., Correia, V., Loureiro, C., Santana, P., 2008. Chronology of the sedimentary processes during the postglacial sea level rise in two estuaries of the Algarve coast, southern Portugal. Estuar. Coast. Shelf Sci. 77, 230–244. https://doi.org/10.1016/j.ecss.2007.09.012.
Bray, E.E., Evans, E.D., 1961. Distribution of n-paraffins as a clue to recognition of source beds. Geochim. Cosmochim. Acta 22 (1), 2–15. https://doi.org/10.1016/0016-7037(61)90069-2.
Brito, P., 2009. Impactos da elevação do nível médio do mar em ambientes costeiros: o caso do estuário do Sado. PhD thesis. In: Departamento de Geologia da Faculdade de Ciências. Universidade de Lisboa, Portugal.
Cabral, H., 1997. Ictiofauna do Estuário do Sado. Relatórios Científicos e Técnicos (47). In: Instituto de Investigação das Pescas e do Mar.
Cabral, M.C., Freitas, M.C., Andrade, C., Cruces, A., 2006. Coastal evolution and Holocene ostracods in Melides lagoon (SW Portugal). Mar. Micropaleontol. 60, 181–204. https://doi.org/10.1016/j.marmicro.2006.04.003.
Camacho, S., Boski, T., Moura, D., Scott, D., Connor, S., Pereira, L., 2016. Paleoenvironmental evolution of the Guadiana Estuary, Portugal, during the Holocene: a modern foraminifera analog approach. The Holocene 27 (2), 197–235. https://doi.org/10.1177/0959683616658526.
Cambourieu-Nebout, N., Peyron, O., Dormoy, I., 2009. Rapid climatic variability in the West Mediterranean during the last 25 000 years from high resolution pollen data. Clim. Past 5, 503–521. https://doi.org/10.5194/cpd-5-671-2009.
Carvalho, A.F., 2009. O Mesolítico Final em Portugal. El Mesolítico Geométrico en la Península Ibérica, Monografías Arqueológicas 44, 33–68.
Chabaud, L., Goñi, M.F.S., Desprat, S., Rossignol, L., 2015. Land – sea climatic variability in the eastern North Atlantic subtropical region over the last 14,200 years: Atmospheric and oceanic processes at different timescales. The Holocene 24, 787–797. https://doi.org/10.1177/0959683614530439.
Chaumillon, E., Tessier, B., Reynaud, J.-Y., 2010. Stratigraphic records and variability of incised valleys and estuaries along French coasts. Bull. Soc. Geol. Fr. 181 (2), 75–85. https://doi.org/10.2113/gssgfbull.181.2.75.
Coleman, M., Meier-Augenstein, W., 2014. Ignoring IUPAC guidelines for measurement and reporting of stable isotope abundance values affects us all. Letter to the Editor, Rapid Commun. Mass Spect. 28, 1953–1955.
Connolly, R.M., Gorman, D., Hindell, J.S., Kildea, T.N., Schlacher, T.A., 2013. High congruence of isotope sewage signals in multiple marine taxa. Mar. Pollut. Bull. 71, 152–158. https://doi.org/10.1016/j.marpolbul.2013.03.021.
Costa, A.M., Freitas, M.C., Leira, M., Costas, S., Costa, P.J.M., Andrade, C., Bao, R., Duarte, J., Rodrigues, A., Cachão, M., Araújo, A.C., Diniz, M., Arias, P., 2019. The role of climate, marine influence and sedimentation rates in late Holocene estuarine evolution (SW Portugal). The Holocene 29, 622–632. https://doi.org/10.1177/0959683618824768.
Costa, A.M., Freitas, M.C., Mota, R., Leira, M., Andrade, C., Pimentel, N., Araújo, A.C., Bao, R., Diniz, M., Arias, P., 2020. Sado palaeovalley configuration: Implications for the Mesolithic settlement during the Holocene Sea-level rise. In: Roque, A., Brito, C., Veracini, C. (Eds.), People, Nature and Environments: Learning to Live Together. Part 4 - Landscape and Heritage, Chapter Thirteen. Cambridge Scholars Publishing, pp. 176–194.
Costa, A.M., Freitas, M.C., Leira, M., Fonseca, R., Duarte, J., Diniz, M., Arias, P., 2021. Late Holocene evolution of a Mediterranean incised valley: Sedimentary dynamics, fluvial activity and palaeoenvironmental reconstruction (SW Iberia). Quat. Int. https://doi.org/10.1016/j.quaint.2021.12.002 submitted (online early).
Costas, S., Rebêlo, L., Brito, P., Fitzgerald, D., 2015. The Joint history of Tróia Península and Sado Ebb-Delta. In: Randazzo, G., Jackson, D.W.T., Cooper, J.A.G. (Eds.), Sand and Gravel Spit. Spinger, pp. 79–102.
Costas, S., Ferreira, O., Plomaritis, T.A., Leorri, E., 2016. Coastal barrier stratigraphy for Holocene high-resolution sea-level reconstruction. Sci. Rep. 6, 38726.
Crann, C.A., Murseli, S., St-Jean, G., Zhao, X., Clark, I.D., Kieser, W.E., 2017. First status report on radiocarbon sample preparation at the a.E. Lalonde AMS Laboratory (Ottawa, Canada). Radiocarbon 59, 695–704. https://doi.org/10.1017/RDC.2016.55.
Cunha, A.H., Erzini, K., Serrão, E.A., Gonçalves, E., Borges, R., Henriques, M., Guerra, M., Duarte, C., Marbá, N., Fonseca, M., 2014. Biomares, a LIFE project to restore and manage the biodiversity of Prof. Luiz Saldanha Marine Park. J. Coast. Conserv. 18 (6), 643–655. https://www.jstor.org/stable/i24760666.
Dabrio, C.J., Zazo, C., Goy, J.L., Sierro, F.J., Borja, F., Lario, J., González, J.A., Flores, J. A., 2000. Depositional history of estuarine infill during the last postglacial transgression (Gulf of Cadiz, Southern Spain). Mar. Geol. 162, 381–404. https://doi.org/10.1016/S0025-3227(99)00069-9.
Debenay, J.-P., 2012. A Guide to 1,000 Foraminifera from Southwestern Pacific: New Caledonia. Marseille, IRD Editions.
Dias, J.M., Boski, T., Rodrigues, A., Magalhães, F., 2000. Coast line evolution in Portugal since the last Glacial Maximum until presente - a synthesis. Mar. Geol. 170, 177–186. https://doi.org/10.1016/S0025-3227(00)00073-6.
Diniz, M., Arias, P., 2012. O povoamento humano do paleo-estuário do Sado (Portugal): Problemáticas em torno da ocupação dos concheiros Mesolíticos. In: Almeida, A.C., Bettencourt, A.M.S., Moura, D., Monteiro-Rodrigues, S., Alves, M.I.C. (Eds.), Mudanças ambientais e interação humana na fachada atlântica ocidental. Coimbra, APEQ/CITCEM/CEGT/CGUP/CCT, pp. 139–157.
Duarte, C., Iriarte, E., Diniz, M., Arias, P., 2019. The microstratigraphy record of human activities and formation processes at the Mesolithic Shell midden of Poças de São Bento (Sado Valley, Portugal). Archaeol. Anthropol. Sci. 11, 483–509. https://doi.org/10.1007/s12520-017-0519-0.
Elfadly, A.A., Ahmed, O.E., El Nady, M.M., 2017. Assessing of organic content in surface sediments of Suex Gulf, Egypt depending on normal alkanes, terpanes and steranes biological markers indicators. Egypt. J. Pet. 26, 969–979. https://doi.org/10.1016/j.ejpe.2016.11.007.
Fatela, F., Taborda, R., 2002. Confidence limits of species proportions in microfossil assemblages. Mar. Micropaleontol. 45, 169–174. https://doi.org/10.1016/S0377-8398(02)00021-X.
Fatela, F., Moreno, J., Antunes, C., Leorri, E., Taborda, R., Silva, A., Andrade, C., Cearreta, A., 2009. Foraminiferal assemblages distribution across the Sado estuary tidal marshes (SW Portugal): local assessment of regional palaeoenvironmental value, 6° Simpósio sobre el Margen Ibérico Atlántico, MIA 2009. Oviedo 345–348.
Ficken, K.J., Li, B., Swain, D.L., Eglinton, G., 2000. An n-alkane proxy for the sedimentary input of submerged/floating freshwater aquatic macrophytes. Org. Geochem. 31 (7), 745–749. https://doi.org/10.1016/S0146-6380(00)00081-4.
Flemming, B., 2000. A revised textural classification of gravel-free muddy sediments on the basis of ternary diagrams. Cont. Shelf Res. 20, 1125–1137. https://doi.org/10.1016/S0278-4343(00)00015-7.
Fletcher, W.J., Sánchez Goñi, M.F., 2008. Orbital- and sub-orbital-scale climate impacts on vegetation of the western Mediterranean basin over the last 48,000 yr. Quat. Res. 70, 451–464. https://doi.org/10.1016/j.yqres.2008.07.002.
Fletcher, W., Boski, T., Moura, D., 2007. Palynological evidence for environmental and climatic change in the lower Guadiana valley, Portugal, during the last 13000 years. The Holocene 17 (4), 481–494. https://doi.org/10.1177/0959683607077027.
Fontanals-Coll, M., Subirà, M.E., Marín-Moratalla, N., Ruiz, J., Gibaja, J.F., 2014. From Sado Valley to Europe: Mesolithic dietary practices through different geographic distributions. J. Archaeol. Sci. 50, 539–550. https://doi.org/10.1016/j.jas.2014.07.028.
Freitas, M.C., Andrade, C., Cruces, A., 2002. The geological record of environmental changes in southwestern Portuguese coastal lagoons since the Lateglacial. Quat. Int. 93-94, 161–170. https://doi.org/10.1016/S1040-6182(02)00014-9.
Freitas, M.C., Andrade, C., Rocha, F., Tassinari, C., Munhá, J.M., Cruces, A., Vidinha, J., Marques da Silva, C., 2003. Lateglacial and Holocene environmental changes in Portuguese coastal lagoons 1: the sedimentological and geochemical records of the Santo André coastal area. The Holocene 13 (3), 433–446. https://doi.org/10.1191/0959683603hl636rp.
Gabriel, S., Prista, N., Costa, M.J., 2012. Estimating meagre (*Argyrosomus regius*) size from otoliths and vertebrae. J. Archaeol. Sci. 39, 2859–2865. https://doi.org/10.1016/j.jas.2012.04.046.
García-Artola, A., Stephan, P., Cearreta, A., Kopp, R.E., Khan, S.N., Horton, B.P., 2018. Holocene Sea-level database from the Atlantic coast of Europe. Quat. Sci. Rev. 196, 177–192. https://doi.org/10.1016/j.quascirev.2018.07.031.
Golubkov, M.S., Nikulina, V.N., Tiunov, A.V., Golubkov, S.M., 2020. Stable C and N isotope composition of suspended particulate organic matter in the Neva estuary: the role of abiotic factors, productivity, and phytoplankton taxonomic composition. J. Marine Sci. Eng. 8, 959. https://doi.org/10.3390/jmse120959.
Gomes, S.D., Fletcher, W.J., Rodrigues, T., Stone, A., Abrantes, F., Naughton, F., 2020. Time-transgressive Holocene maximum of temperate and Mediterranean forest development across the Iberian Peninsula reflects orbital forcing. Palaeogeogr.

Palaeoclimatol. Palaeoecol. 550, 109739 https://doi.org/10.1016/j.palaeo.2020.109739.
Gonçalves, F., Antunes, M.T., 1992. Notícia explicativa da Folha 39-D Torrão, Carta Geológica de Portugal 1:50000. Serviços Geológicos de Portugal, Lisboa.
Gu, B., 2009. Variations and controls of nitrogen stable isotopes in particulate organic matter of lakes. Oecologia 160, 421–431. https://doi.org/10.1007/s00442-009-1323-z.
Gutiérrez-Zugasti, I., Andersen, S.H., Araújo, A.C., Dupont, C., Milner, N., Monge-Soares, A.M., 2011. Shell midden research in Atlantic Europe: State of the art, research problems and perspectives for the future. Quat. Int. 239, 70–85. https://doi.org/10.1016/j.quaint.2011.02.031.
Hijma, M.P., Cohen, K.M., Hoffmann, G., Van der Spek, A.J.F., Stouthamer, E., 2009. From river valley to estuary: the evolution of the Rhine mouth in the early to middle Holocene (western Netherlands, Rhine-Meuse delta). Neth. J. Geosci. 88 (1), 13–53. https://doi.org/10.1017/S0016774600000986.
Hughes, W.B., Holba, A.G., Dzou, I.P., 1995. The ratios of dibenzothiophene to phenanthrene and pristana to phytane as indicatiors of depositional environment and lithology of petroleum source rocks. Geochim. Cosmochim. Acta 59 (17), 3581–3598. https://doi.org/10.1016/0016-7037(95)00225-O.
INE, 2007. Anuário Estatístico da Região do Alentejo. Lisboa, INE.
Jarzen, D.M., Elsik, W.C., 1986. Fungal palynomorphs recovered from recent river deposits, Luangwa valley, Zambia. Palynology 10, 35–60. https://doi.org/10.1080/01916122.1986.9989302.
Khan, N.S., Vane, C.H., Horton, B.P., 2015. Stable carbon isotope and C/N geochemistry of coastal wetland sediments as a sea-level indicator. In: Shennan, I., Long, A.J., Horton, B.P. (Eds.), Handbook of Sea-Level Research, 1st edition. John Wiley & Sons, Ltd, pp. 295–311.
Kopprio, G.A., Dutto, M.S., Garzón Cardona, J.E., Gärdes, A., Lara, R.J., Graeve, M., 2018. Biogeochemica markers across a pollution gradient in a Patagonian estuary: a multidimensional approach of fatty acids and stable isotopes. Mar. Pollut. Bull. 137, 617–626. https://doi.org/10.1016/j.marpolbul.2018.10.059.
Kristensen, E., 1990. Characterization of biogenic organic matter by stepwise thermogravimetry (STG). Biogeochemistry 9, 135–159. https://doi.org/10.1007/BF00692169.
Laermanns, H., Pint, A., Bellanova, P., Feist, L., Wagner, B., Frank, S., Mathes-Schmidt, M., Scheder, J., Teichner, F., Reicherter, K., Brückner, H., 2021. The Santo André lagoon at the Atlantic coast of Portugal - Holocene evolution and event history. Paleogeogr. Palaeoclimatol. Palaeoecol. 571, 110366 https://doi.org/10.1016/j-palaeo.2021.110366.
Lamb, A.L., Wilson, G.P., Leng, M.J., 2006. A review of coastal palaeoclimate and relate sea-level reconstructions using $\delta^{13}C$ and C/N rations in organic material. Earth Sci. Rev. 75, 29–57. https://doi.org/10.1016/j.earscirev.2005.10.003.
Lario, J., Zazo, C., Goy, J.L., Dabrio, C.J., Borja, F., Silva, P.G., Sierro, F., González, A., Soler, V., Yll, E., 2002. Changes in sedimentation trends in SW Iberia Holocene estuaries (Spain). Quat. Int. 93–94, 171–176. https://doi.org/10.1016/S1040-6182(02)00015-0.
Laussaque, J., Lepoint, G., Thibaut, T., Francour, P., Meinesz, A., 2010. Tracing sewage and natural freshwater input in a Northwest Mediterranean bay: evidence obtained from isotopic ratios in marine organisms. Mar. Pollut. Bull. 60, 843–851. https://doi.org/10.1016/j.marpolbul.2010.01.008.
Leorri, E., Cearreta, A., Milne, G., 2012. Field observations and modelling of Holocene Sea-level changes in the southern Bay of Biscay: implications for understanding current rates of relative sea-level change and vertical land motion along the Atlantic coast of SW Europe. Quat. Sci. Rev. 42, 59–73. https://doi.org/10.1016/j.quascirev.20212.03.014.
Lepoint, G., Dauby, P., Gobert, S., 2004. Applications of C and N stable isotopes to ecological and environmental studies in seagrass ecosystems. Mar. Pollut. Bull. 49, 887–891. https://doi.org/10.1016/j.marpolbul.2004.07.005.
Li, Z., Sun, Y., Nie, X., 2020. Biomarkers as a soil organic carbon tracer of sediment: recent advances and challenges. Earth Sci. Rev. 208, 103277 https://doi.org/10.1016/j.earscirev.2020.103277.
Loeblich Jr., A.R., Tappan, H., 1988. Foraminiferal Genera and their Classification. Van Nostrand Reinhold Company, New York.
López-Sáez, J.A., van Geel, B., Martín Sánchez, M., 2000. Aplicación de los microfósiles no polínicos en Palinología Arqueológica. Contributos das Ciências e das. Tecnologias para a Arqueologia da Península Ibérica. Actas 3° Congresso de Arqueologia Peninsular IX. Adecap, Porto, pp. 11–20.
Meyers, P.A., 1994. Preservation of elemental and isotopic source identification of sedimentary organic matter. Chem. Geol. 144, 289–302. https://doi.org/10.1016/0009-2541(94)90059-0.
Meyers, P.A., 2003. Applications of organic geochemistry to paleolimnological reconstructions: a summary of examples from the Laurentian Great Lakes. Org. Geochem. 34, 261–289. PII: S0146-6380(02)00168–7.
Miola, A., 2012. Tools for Non-Pollen Palynomorphs (NPPs) analysis: a list of Quaternary NPP Types and Reference Literature in English Language (1972–2011). Rev. Palaeobot. Palynol. 186, 142–161. https://doi.org/10.1016/j.revpalbo.2012.06.010.
Mita, H., Shimoyama, A., 1999. Characterization of n-alkanes, pristine and phytane in the cretaceous/Tertiary boundary sediments at Kawaruppu, Hokkaido, Japan. Geochem. J. 33, 285–294. https://www.jstage.jst.go.jp/article/geochemj1966/33/5/33_5_285/_pdf.
Moore, P.D., Webb, J.A., Collinson, M.E., 1991. Pollen Analysis. Blackwell Scientific Publications, Oxford.
Moreno, J., Valente, T., Moreno, F., Fatela, F., Guise, L., Patinha, C., 2007. Occurrence of calcareous foraminifera and calcite-carbonate equilibrium conditions - a case study in Minho/Coura estuary (Northern Portugal). Hydrobiologia 587, 177–184. https://doi.org/10.1007/s10750-007-0677-7.
Murray, J.W., 2006. Ecology and Applications of Benthic Foraminifera. Cambridge University Press, London, pp. 7–26.
Murray, J.W., 2007. Biodiversity of living benthic foraminifera: how many species are there? Mar. Micropaleontol. 64, 163–176. https://doi.org/10.1016/j.marmicro.2007.04.002.
Ouyang, X., Guo, F., Bu, H., 2015. Lipid biomarkers and pertinent indices from aquatic environment record paleoclimate and paleoenvironment changes. Quat. Sci. Rev. 123, 180–192. https://doi.org/10.1016/j.quascirev.2015.06.029.
Pals, J.P., van Geel, B., Delfos, A., 1980. Paleoecological studies in the Klokkeweel bog near Hoogkarspel (Prov. Of Noord-Holland). Rev. Palaeobot. Palynol. 30, 371–418. https://doi.org/10.1016/0034-6667(80)90020-2.
Peyroteo-Stjerna, R., 2020. Chronology of the burial activity of the last hunter-gatherers in the southwestern Iberian Peninsula, Portugal. Radiocarbon 63 (1), 265–299. https://doi.org/10.1017/RDC.2020.100.
Pimentel, N.L., 2002. Pedogenic and early diagenetic processes in Palaeogene alluvial fan and lacustrine deposits from the Sado Basin (S Portugal). Sediment. Geol. 148 (1–2), 123–138. https://doi.org/10.1016/S0037-0738(01)00213-5.
Powell, T.G., 1988. Pristane/phytane ratio as environmental indicator. Nature 333, 604.
Reille, M., 1992. Pollen et Spores d'Europe et d'Afrique du nord. Marseille, Laboratoire de Botanique Historique et Palynologie, CNRS.
Reille, M., 1995. Pollen et Spores d'Europe et d'Afrique du Nord (Supplément 1). Marseille, Laboratoire de Botanique Historique et Palynologie, CNRS.
Reimer, P., Austin, W., Bard, E., Bayliss, A., Blackwell, P., Bronk Ramsey, C., Butzin, M., Cheng, H., Edwards, R., Friedrich, M., Grootes, P., Guilderson, T., Hajdas, I., Heaton, T., Hogg, A., Hughen, K., Kromer, B., Manning, S., Muscheler, R., Palmer, J., Pearson, C., van der Plicht, J., Reimer, R., Richards, D., Scott, E., Southon, J., Turney, C., Wacker, L., Adolphi, F., Büntgen, U., Capano, M., Fahrni, S., Fogtmann-Schulz, A., Friedrich, R., Köhler, P., Kudsk, S., Miyake, F., Olsen, J., Reinig, F., Sakamoto, M., Sookdeo, A., Talamo, S., 2020. The IntCal20 Northern Hemisphere radiocarbon age calibration curve (0–55 cal kBP). Radiocarbon 62. https://doi.org/10.1017/RDC.2020.41.
Santos, C.S., 2019. Estado atual das populações de berbigão (*Cerastoderma* spp.) no estuário do Sado. In: Mestrado em Ecologia e Gestão Ambiental, Faculdade de Ciências da Universidade de Lisboa.
Scanes, P., Ferguson, A., Potts, J., 2019. Estuary Form and Function: Implications for Palaeoecological Studies. In: Weckström, K., Saunders, K.M., Gell, P.A., Skilbeck, C. G. (Eds.), Applications of Paleoenvironmental Techniques in Estuarine Studies. Part I, Estuaries and Their, Management. Springer Nature, pp. 9–44.
Schubel, J.R., 1982. Estuarine sedimentation. In: Schwartz, M. (Ed.), Beaches and Coastal Geology. Encyclopedia of Earth Science. Springer, Boston, MA.
Scott, L., 1992. Environmental implications and origin of microscopic Pseudoschizaea Thiergart and Frantz ex R. Potonie emend. In sediments. J. Biogeogr. 19 (4), 349–354. https://doi.org/10.2307/2845562.
Shannon, C.E., 1948. A mathematical theory of communication. Bell Syst. Tech. J. 27, 379–423.
Sikes, E.L., Uhle, M.E., Nodder, S.D., Howard, M.E., 2009. Sources of organic matter in a coastal marine environment: evidence from n-alkanes and their $\delta^{13}C$ distributions in the Hauraki Gulf, New Zeland. Mar. Chem. 113, 149–163. https://doi.org/10.1016/j.marchem.2008.12.003.
Silliman, J.E., Meyers, P.A., Bourbonniere, R.A., 1996. Record of postglacial organic matter delivery and burial in sediments of Lake Ontario. Org. Geochem. 24, 463–472. https://doi.org/10.1016/0146-6380(96)00041-1.
Sobral, D.V., 1993. Peixes do estuário do Sado. Estudos de Biologia e Conservação da Natureza, 11.
Stockmarr, J., 1971. Tablets with spores used in absolute pollen analysis. Pollen Spores 13, 614–621.
Taborda, R., Freire, P., Silva, A., Andrade, C., Freitas, C., 2009. Origin and evolution of Tagus estuarine beaches. J. Coast. Res. SI56, ICS 2009 Proc. 213–217.
Teixeira, S.B., Gaspar, P., Rosa, M., 2005. Holocene Sea-level index points on the Quarteira coast (Algarve, Portugal). Iberian coastal Holocene paleoenvironmental evolution. Proc. COASTAL HOPE 2005, 125–127.
Teranes, J.L., Bernasconi, S.M., 2000. The record of nitrate utilization and productivity limitation provided by $\delta^{15}N$ values in lake organic matter - a study of sediment trap and core sediments from Baldeggersee, Switzerland. Limnol. Oceanogr. 45 (4), 801–813.
Torres, I.C., Inglett, P.W., Brenner, M., Kenney, F., Reddy, K.R., 2012. Stable isotope ($\delta^{13}C$ and $\delta^{15}N$) values of sediment organic matter in subtropical lakes of different trophic status. J. Palaeolimnol. 47, 693–706. https://doi.org/10.1007/s10933-012-9593-6.
Tweddle, J.C., Edwards, K.J., Fieller, N.R.J., 2005. Multivariate statistical and other approaches for the separation of cereal from wild Poaceae pollen using a large Holocene dataset. Veg. Hist. Archaeobotany 14, 15–30. https://doi.org/10.1007/s00334-005-0064-0.
Umbelino, C., Cunha, E., 2012. The Sado shell middens: Anthropological and paleodietary depiction. In: Gibaja, J.F., Carvalho, A.F., Chambom, P. (Eds.), Funerary Practices in the Iberian Peninsula from the Mesolithic to the Chalcolithic. BAR International Series 2417, pp. 91–102.
Valente, T., Fatela, F., Moreno, J., Guise, L., Patinha, C., 2009. A comparative study of the influence of geochemical parameters on the distribution of foraminiferal assemblages in two distinctive tidal marshes. J. Coast. Res. SI 56, 1439–1443.
van der Schriek, T., Passmore, D.G., Stevenson, A.C., Rolão, J., 2007. The paleogeography of Mesolithic settlement-subsistence and shell midden formation in the Muge valley, lower Tagus Basin, Portugal. The Holocene 17 (3), 369–385. https://doi.org/10.1177/0959683607075839.

van der Schriek, T., Passmore, D.G., Mugica, F.F., Stevenson, A.C., Boomer, I., Rolão, J., 2008. Holocene palaeoecology and floodplain evolution of the Muge tributary, lower Tagus Basin, Portugal. Quat. Int. 189, 135–151. https://doi.org/10.1016/j.quaint.2007.09.007.

van Geel, B., 1978. A palaeoecological study of Holocene peat bog sections in Germany and the Netherlands, based on the analysis of pollen, spores and macro- and microscopic remains of fungi, algae, cormophytes and animals. Rev. Palaeobot. Palynol. 25, 1–120.

van Geel, B., 1986. Application of fungal and algal remains and other microfossils in palynological analyses. In: Berglund, B.E. (Ed.), Handbook of Holocene Palaeoecology and Palaeohydrology. John Wiley & Sons Ltd, pp. 497–505 (Chichester).

van Geel, B., 1992. Fungal Spores as Extra Indicators for Human Impact in the Past? Abstracts 8th International Palynological Congress, Aix-en-Provence.

van Geel, B. (Ed.), 2006. Rev. Palaeobot. Palynol. 141, 1–2.

van Geel, B., Bohncke, S.J.P., Dee, H., 1981. A palaeoecological study of an upper late Glacial and Holocene sequence from "De Borchert", the Netherlands. Rev. Palaeobot. Palynol. 31, 367–448.

van Geel, B., Coope, G.R., van der Hammen, T., 1989. Palaeoecology and stratigraphy of the Lateglacial type section at Usselo (the Netherlands). Rev. Palaeobot. Palynol. 60, 25–129.

van Geel, B., Buurman, J., Brinkkemper, O., Schelvis, J., Aptroot, A., van Reenen, G., Hakbijl, T., 2003. Environmental reconstruction of a Roman Period settlement site in Uitgeest (the Netherlands), with specific reference to coprophilous fungi. J. Archaeol. Sci. 30, 873–883. https://doi.org/10.1016/S0305-4403(02)00265-0.

van Geel, B., Dale Guthrie, R., Altmann, J.G., Broekens, P., Bull, I.D., Gill, F.L., Jansen, B., Nieman, A.M., Gravendeel, B., 2011. Mycological evidence of coprophagy of an Alaskan late Glacial Mammoth. Quat. Sci. Rev. 30 (17–18), 2289–2303. https://doi.org/10.1016/j.quascirev.2010.03.008.

Vis, G.-J., Kasse, C., Vandenberghe, J., 2008. Late Pleistocene and Holocene palaeogeography of the lower Tagus Valley (Portugal): effects of relative sea level, valley morphology and sediment supply. Quat. Sci. Rev. 27, 1682–1709. https://doi.org/10.1016/j.quascirev.2008.07.003.

Vis, G.-J., Bohncke, S.J.P., Schneider, H., Kasse, C., Coenraads-Nederveen, S., Zuurbier, K., Rozema, J., 2010. Holocene flooding history of the lower Tagus Valley (Portugal). J. Quat. Sci. 25 (8), 1222–1238. https://doi.org/10.1002/jqs.1401.

Wang, J.-Z., Ni, H.-G., Guan, Y.-F., Zeng, E.Y., 2008. Occurrence and mass loadings of n-alkanes in riverine runoff of the Pearl River Delta, South China: Global implications for levels and inputs. Environ. Toxicol. Chem. 27 (10), 2036–2041. https://doi.org/10.1897/08-034.1.

Whitlock, C., Larsen, C., 2001. Charcoal as a Fire Proxi. In: Smol, J.P., Birks, H.J.B., Last, W.M., Bradley, R.S., Alverson, K. (Eds.), Tracking Environmental Change using Lake Sediments. Developments in Paleoenvironmental Research, vol 3. https://doi.org/10.1007/0-306-47668-1.

Wilson, G.P., Lamb, A.L., Leng, M.J., Gonzalez, S., Huddart, D., 2005. $\delta^{13}C$ and C/N as potential coastal palaeoenvironmental indicators in the Mersey Estuary, UK. Quat. Sci. Rev. 24, 2015–2029. https://doi.org/10.1016/j.earscirev.2005.10.003.

Yamamuro, M., Kayanne, H., Yamano, H., 2003. $\delta^{15}N$ of seagrass leaves for monitoring anthropogenic nutrient increases in coral reef ecosystems. Mar. Pollut. Bull. 46, 452–458. https://doi.org/10.1016/S0025-326X(02)00463-0.

Zilhão, J., 2004. Muge shell middens. In: Bogucki, P., Crabtree, P.J. (Eds.), Ancient Europe 8000 B.C. - A.D. 1000: Encyclopedia of the Barbarian World, vol. I. Charles Scribner's Sons, New York, pp. 164–166.